AD NUMBER

AD433214

LIMITATION CHANGES

TO:

Approved for public release; distribution is unlimited. Document partially illegible.

FROM:

**Distribution authorized to U.S. Gov't. agencies and their contractors;
Administrative/Operational Use; FEB 1964. Other requests shall be referred to Office of Naval Research, Arlington, VA 22203. Document partially illegible.**

AUTHORITY

ONR ltr dtd 15 Jun 1977

TR-EE 64-5
OFFICE OF NAVAL RESEARCH CONTRACT Nonr-1100(24)

PURDUE UNIVERSITY
SCHOOL OF ELECTRICAL ENGINEERING

D. C. Polarization in a Nonlinear Dielectric Medium at Optical Frequencies

A. K Kamal
and
M. Subramanian

Quantum Electronics Laboratory

February, 1964
Lafayette, Indiana

SUPPORTED BY
OFFICE OF NAVAL RESEARCH
WASHINGTON D.C.

D. C. POLARIZATION IN A NONLINER DIELECTRIC MEDIUM AT OPTICAL FREQUENCIES*

FIRST SEMI-ANNUAL
TECHNICAL SUMMARY REPORT

December 31, 1963

Prepared for

THE OFFICE OF NAVAL RESEARCH

on

Contract No. Nonr–1100(24)
Project Code 015–803
ARPA Order No. 306–62

by

A. K. Kamal
and
M. Subramanian

Quantum Electronics Laboratory

School of Electrical Engineering
Purdue University
Lafayette, Indiana

Period covered

April 1 through December 31, 1963

* This research is a part of Project DEFENDER, under the joint sponsorship of the Advanced Research Projects Agency, the Office of Naval Research and the Department of Defense.

TABLE OF CONTENTS

TABLE OF CONTENTS (Continued)

LIST OF ILLUSTRATIONS

LIST OF ILLUSTRATIONS (Continued)

ABSTRACT

Subramanian, Mahadevan, Ph. D., Purdue University, January, 1964. D. C. Polarization in a Nonlinear Dielectric Medium at Optical Frequencies. Major Professor: Aditya K. Kamal.

Investigation of nonlinear properties of materials at optical frequencies has been made possible with the development of high power lasers. One of the nonlinearities encountered is the second order polarization in dielectric media that lack inversion symmetry. The second order nonlinear polarization gives rise to generation of second harmonic and d.c. components. The scope of this thesis concerns with the latter phenomenon.

The quartz crystal is chosen as the dielectric medium. A quantitative relationship between the d. c. polarization and the intensity of the propagating laser beam is developed by following a phonomenological approach. A convenient method of detecting the d. c. polarization is presented. With this technique the elements of second order polarization coefficient tensor can be determined experimentally. The second order polarization term is responsible for transferring energy from the fundamental to the second harmonic. It is shown that it cannot, however, transfer any energy to the d. c. component. Thus, optical power rectification is not possible.

By considering a suitable detecting system with a convenient configuration of the quartz crystal, it is shown that the output voltage

of the detector is linearly proportional to the intensity of the laser pulse. Thus the possibility of using this principle to build a transmission type of meter for measuring power in high power laser pulses is presented.

Some of the theoretical results have been proved by experiments. One of the two elements in the second order nonlinear polarization coefficient tensor has been shown experimentally to be in the order of 10^{-8} e. s. u. Also the linear relationship between the detector output and the laser intensity is verified, confirming the feasibility of applying this principle for laser power measurement.

INTRODUCTION

The advent of laser has initiated great interest in the investigation of the nonlinear properties of materials at optical frequencies. The laser is claimed to have many potential applications some of which use the nonlinear properties of materials. These nonlinearities though may be insignificant at the ordinary power levels that were hitherto encountered, are brought to perceivable significance by high power laser beams. In an unfocused beam of a pulsed ruby laser one can now obtain power in the order of megawatts and higher. This can be increased further by orders of magnitude with the help of external Q-switching arrangements.

One of the nonlinear properties of a material that came into early observation is its dielectric property. The nonlinear susceptibilities have already been used for mixing and harmonic generation [1, 2, 3]. The observation by Franken, et. al [1] of the second harmonic by passing ruby laser beam through crystals that lack inversion symmetry motivated interest in the investigation of the d. c. polarization that should accompany the second harmonic generation. After the preliminary analysis and experiment with quartz crystal gave positive indication of the existence of d. c. polarization the project was continued with the following objectives.

1) To establish firmly the existence of the d. c. polarization. Bass, et. al [4] have since reported observing the d. c. polarization.

ii) To estimate the second order nonlinear polarization coefficient tensor for quartz crystal.

iii) To investigate the feasibility of applying this phenomenon for laser power measurement.

The concept of d.c. polarization is developed in the early part of Chapter 1. The rest of the chapter is devoted to a brief review of the earlier work done in the field.

Since the conventional approach of propagation of electromagnetic wave in a medium does no longer apply for the degenerate case of d.c, a simple method of analyzing the d.c. part is presented for the specific case of quartz crystal medium in Section 2.1. The angular dependence of the d.c. polarization on the polarization direction of the radiation field is presented in Section 2.2. This is an important result in the experimental confirmation of the phenomenon of d.c. polarization. Many crystals that develop d.c. polarization have non-zero pryroelectric coefficient. In the experimental observation one has to distinguish carefully between these two components. Whereas the pyroelectric voltage is developed in a unique direction, the d.c. polarization, as shown in Section 2.2, has a cos 2θ variation when the crystal is rotated about its axis. Section 2.3 proves that no energy conversion is possible using this principle, even though the d.c. polarization resembles rectification in the electrical circuits.

Chapter 3 serves the purpose of explaining the interaction between the d.c. field set up by the propagating laser beam and the detecting circuitry. A simplified model of a parallel plate capacitor is chosen and the equivalent circuit of the model is derived. The fact that the

system cannot deliver any d.c. power is confirmed from the circuitry point of view. However, the possibility of low frequency intensity modulation detection is explained.

The ruby laser output beam is normally circular in cross-section. For high power operation it is pulsed, and one often needs to know the exact intensity of the laser pulse which is being used for some external application. Thus a transmission-type of power meter would prove more beneficial than either the calorimetric techniques which measure only energy or the photodetecting devices which need periodic calibration. The application of the nonlinear d.c. polarization to power and energy measurement is described in detail in Chapter 4. The theory is presented and a practical model is suggested. It is shown that the output of such a device will indicate directly the power content in the laser beam.

The construction of the quartz detector mount and the experimental arrangements and results are given in Chapter 5. Summary and conclusions are presented in Chapter 6.

Chapter 1

REVIEW OF EARLIER WORK

Although considerable progress has been made in the field of nonlinear optics both in theory and experiment on generation of harmonics, electro-optic effect in solids and liquids, etc., not much has been reported on the d.c. polarization. Franken and Ward [5] have presented a good summary on nonlinear optics in their review article. In this chapter the concept of d.c. polarization is developed by assuming a simple mathematical model. It is followed by a review of the theoretical work that has been done on the phenomenon of d.c. polarization.

1.1. D. C. Polarization in a Nonlinear Dielectric Medium

The phenomenon of d.c. polarization can be easily explained by assuming a scalar mathematical model for the polarization. Consider an electromagnetic wave propagating through a nonlinear medium. In the scalar form, the polarization p may be written as a power series in terms of the electric field E that gives rise to it.

$$p = a_1 E + a_2 E^2 + a_3 E^3 + \cdots \qquad (1.1)$$

where a_1, a_2, a_3, ... are called the first, second, third, ... order polarization coefficients. In writing Eq. (1.1), the gradients of the E field have been neglected for simplicity. Writing the radiation field intensity $E = E_0 \cos \omega t$ in Eq. (1.1), one has

$$p = a_1 E_o \cos \omega t + \frac{a_2}{2} E_o^2 (1 + \cos 2\omega t) + \frac{a_3}{4} E_o^3 (3 \cos \omega t + \cos 3\omega t) + \cdots \quad (1.2)$$

The first term in the right hand side of Eq. (1.2) represents the linear polarization and has the same frequency as the inducing field. The second term on the right hand side generates a d.c. component and a second harmonic component. It is observed that the term which is responsible for the second harmonic generation also causes the d.c. polarization. Contributions to d.c. polarization from terms higher than the second order is neglected in the present discussion. In experimentally determining the value of the second order nonlinear coefficient, the d.c. component will be the only part that will be of interest. This is due to the fact that whereas the d.c. polarization depends only on the magnitude of the second order nonlinear coefficient and the power content of the beam, the second harmonic generation is also greatly influenced by the phase matching conditions.

The generalized expression of Eq. (1.1) is of tensor form and also includes the contributions to the polarization due to gradient of the electric field intensity. In the absence of any external biasing electric or magnetic fields the total polarization in a nonlinear dielectric medium due to a propagating electromagnetic wave may be expressed as a power series in terms of the components of the electric field and its gradient.

$$P_i = \epsilon_o \left[\chi^{(1)}_{ij} E_j + \chi^{(2)}_{ijk} \nabla_j E_k + \chi^{(3)}_{ijk} E_j E_k + \chi^{(4)}_{ijkl} E_j \nabla_k E_l \right.$$

$$\left. + \chi^{(5)}_{ijkl} E_j E_k E_l + \cdots \right] \qquad (1.3)$$

where P_i is the i^{th} spatial component of the polarization $\vec{P}$, χ's represent the various orders of polarization coefficient tensors, ∇'s denote the gradient operation, E's are the spatial components of the electric field intensity and ϵ_o the free space permittivity. Franken and Ward [5] have discussed the physical significance of the various terms in Eq. (1.3). It is enough to mention here that the only term in the right hand side that can cause d.c. polarization in a medium is the second order term. The magnitude of d.c. polarization due to terms of higher order than those in Eq. (1.3) can be neglected as compared with that of the second order term since the contribution to polarization decreases as the ratio of the electric field intensity E of the electromagnetic wave to the atomic electric field intensity E_{atomic} (E/E_{atomic}) for each additional E factor added [5]. The symmetry considerations in a crystal that lead to the presence of the second order term will now be discussed.

1.2. Second Order Polarization

It has been shown in the previous section that the only significant term in Eq. (1.3) that contributes to the development of d.c. polarization is the quadratic term. Hence only this term will be considered hereafter. Rewriting Eq. (1.3) with only the second-order term present, one has

$$P_i = \chi_{ijk} E_j E_k \qquad (1.4)$$

In Eq. (1.4) the order of $E_j E_k$ is not physically significant. This facilitates the reduction of the 27 elements of the third rank tensor of Eq. (1.4) to 18 elements due to the symmetry property

$$\chi_{ijk} = \chi_{ikj} \tag{1.5}$$

One can now use the piezoelectric tensor representation [6] and rewrite Eq. (1.4) as

$$p_i = \chi_{ij} S_j \qquad (i = 1, 2, 3;\ j = 1, 2, \ldots, 6) \tag{1.6}$$

where χ_{ij} is the contracted form of χ_{ijk} and S_j's are as defined below

$$S_1 = E_x^2 \ ; \ S_2 = E_y^2 \ ; \ S_3 = E_z^2 \ ; \ S_4 = E_y E_z \ ; \ S_5 = E_x E_z \ ;$$

$$S_6 = E_x E_y$$

It can be shown [5] that $\chi_{ij} = 0$ for crystals that possess an inversion symmetry. This leaves only 21 classes of crystals to be considered. Since χ_{ij} possesses the same symmetry properties that the piezoelectric modulus does, the non-vanishing terms in χ_{ij} are the same as that in the piezoelectric modulus.

Armstrong, et. al. have shown [7] theoretically that the second order polarization tensor is the same as the electro-optic tensor. According to their approach, the local field E_{loc} acting on an atom can be written explicitly in terms of the external electric field E and the fields due to the linear polarization $\vec{P}^L$ and the nonlinear polarization $\vec{P}^{NL}$. Thus

$$\vec{E}_{loc} = \vec{E} + \frac{\vec{P}^{L}}{3\epsilon_0} + \frac{\vec{P}^{NL}}{3\epsilon_0} \tag{1.7}$$

where ϵ_0 is the free space permittivity. The displacement vector D occurring in Maxwell's equations describing a macroscopically isotropic medium is then given by

$$\vec{D} = \epsilon_0 \vec{E} + \vec{P}^{L} + \vec{P}^{NL} \tag{1.8}$$

If the linear polarization is described as

$$\vec{P}^{L} = \epsilon_0 \chi \vec{E}_{loc} \tag{1.9}$$

where χ is the linear polarization coefficient, then it follows from Eqs. (1.7) and (1.9),

$$\vec{P}^{L} = \frac{\epsilon_0 \chi}{1 - \frac{\chi}{3}} \vec{E} + \frac{\chi}{3(1 - \frac{\chi}{3})} \vec{P}^{NL} \tag{1.10}$$

From Maxwell's equation for linear medium

$$\vec{P}^{L} = \epsilon_0(\epsilon_r - 1) \vec{E} \tag{1.11}$$

where ϵ_r is the linear relative dielectric constant. Equating the coefficients of $\vec{E}$ in (1.10) and (1.11), Eq. (1.10) may be rewritten as

$$\vec{P}^{L} = \epsilon_0(\epsilon_r - 1) \vec{E} + \frac{(\epsilon_r - 1)}{3} \vec{P}^{NL} \tag{1.12}$$

From Eqs. (1.8) and (1.12), it can be shown that

$$\vec{D} = \epsilon \vec{E} + \frac{\epsilon_r + 2}{3} \vec{P}^{NL} \tag{1.13}$$

where $\epsilon = \epsilon_o \epsilon_r$. If we define

$$\vec{D} = \epsilon \vec{E} + \vec{P}^{NLS} \tag{1.14}$$

where $\vec{P}^{NLS}$ is the effective nonlinear source of polarization, then from Eqs. (1.13) and (1.14)

$$\vec{P}^{NLS} = \frac{\epsilon_r + 2}{3} \vec{P}^{NL} \tag{1.15}$$

Thus the effective nonlinear polarization source term is $(\epsilon_r + 2)/3$ times the true nonlinear polarization. The latter is calculated from the following relationship [7]

$$\vec{P}^{NL} = \epsilon_o \vec{\vec{\beta}} : \vec{E}_{loc} \vec{E}_{loc} \tag{1.16}$$

where β is a third rank tensor.

The above procedure described for an isotropic medium also holds good for the case of an anisotropic medium. Armstrong, et. al. [7] have proved the following relationship for the latter case.

$$\vec{P}^{NLS}(\omega_3) = \epsilon_o \vec{\vec{\chi}}(\omega_3 = \omega_1 + \omega_2) : \vec{E}_1(\omega_1) \vec{E}_2(\omega_2) \tag{1.17}$$

where $\vec{P}^{NLS}$ is the effective nonlinear polarization developed at the sum frequency of $\omega_3 = \omega_1 + \omega_2$ due to the interaction of two propagating waves with electric field intensities $\vec{E}_1$ at frequency ω_1 and $\vec{E}_2$ at frequency ω_2.

$\vec{\vec{\chi}}$ is again a third rank tensor. It is further shown [7] that the tensor χ_{ijk} in Eq. (1.17) follows the symmetry relationship

$$\chi_{ijk}(\omega_3 = \omega_1 + \omega_2) = \chi_{kij}(\omega_2 = \omega_3 - \omega_1) = \chi_{jik}(\omega_1 = \omega_3 - \omega_2) \qquad (1.18)$$

There are the following two interesting cases of Eqs. (1.17) and (1.18) corresponding to

1) $\omega_3 = \omega_2 = \omega$
   $\omega_1 = 0$

2) $\omega_1 = \omega_3 = \omega$
   $\omega_2 = 0$

$$P_i^{NLS}(0) = \chi_{jik}(0)\, E_i(\omega)\, E_k(\omega) \qquad (1.19)$$

$$P_i^{NLS}(\omega) = \chi_{jik}(\omega)\, E_i(\omega)\, E_k(0) \qquad (1.20)$$

Eq. (1.19) describes the d.c. polarization effect and Eq. (1.20) describes the linear electro-optic effect. The linear electro-optic effect is the change in the dielectric tensor of the medium due to an applied d.c. electric field. From symmetry considerations expressed by Eq. (1.18) and from Eqs. (1.19) and (1.20) it follows that the second order polarization tensor is the same as the linear electro-optic tensor.

Chapter 2

D. C. POLARIZATION IN QUARTZ CRYSTAL

2.1. Propagation of Electromagnetic Wave Through Quartz Medium

The propagation of an electromagnetic wave through a nonlinear medium has already been considered in detail by various authors [7, 8] from both the quantum mechanical veiwpoint and the phenomenalogical approach. While considering the interaction between various waves propagating in the medium, one has to take into consideration such effects as the dispersion in the medium and the phase velocity of each wave component, and so forth. However in the case of d.c. the phase velocity is infinite and there is no propagation of the wave at zero frequency. The approach to the problem becomes different. The following analysis is made for the propagation of an electromagnetic wave through a nonlinear quartz medium by classical methods. It is assumed that the medium is non-dissipative and infinite in extent.

Quartz crystal belongs to class 32; that is, it has a 3 fold symmetry along the z-axis or optic axis and 2 fold symmetry along x-axis. Due to these symmetry considerations, the second order nonlinear coefficient tensor X_{ij} for quartz can be written in the form similar to its piezoelectric tensor [9] which is shown below

$$X_{ij} = \frac{1}{\epsilon_o} \begin{pmatrix} \alpha & -\alpha & 0 & \beta & 0 & 0 \\ 0 & 0 & 0 & 0 & -\beta & -2\alpha \\ 0 & 0 & 0 & 0 & 0 & 0 \end{pmatrix} \qquad (2.1)$$

where α and β are constants. It is evident that there are only two independent elements in the entire matrix. Substituting Eq. (2.1) in Eq. (1.6), one has

$$\begin{pmatrix} p_x \\ p_y \\ p_z \end{pmatrix} = \begin{pmatrix} \alpha & -\alpha & 0 & \beta & 0 & 0 \\ 0 & 0 & 0 & 0 & -\beta & -2\alpha \\ 0 & 0 & 0 & 0 & 0 & 0 \end{pmatrix} \begin{pmatrix} E_x^2 \\ E_y^2 \\ E_z^2 \\ E_y E_z \\ E_z E_x \\ E_x E_y \end{pmatrix} \tag{2.2}$$

Expansion of Eq. (2.2) gives

$$\begin{aligned} p_x &= \alpha(E_x^2 - E_y^2) + \beta E_y E_z \\ p_y &= -\beta E_x E_z - 2\alpha E_x E_y \\ p_z &= 0 \end{aligned} \tag{2.3}$$

If we consider a wave to be propagating along the optic axis of the crystal, then $E_z = 0$ and Eqs. (2.3) reduce to

$$\begin{aligned} p_x &= \alpha(E_x^2 - E_y^2) \\ p_y &= -2\alpha E_x E_y \\ p_z &= 0 \end{aligned} \tag{2.4}$$

It should be noted that no mention has so far been made about the

characteristics of the propagating wave. Thus Eqs. (2.4) are valid for any type of polarization of the propagating wave, elliptical, circular or linear. To take this into account one can express the components of the electric field explicitly by specifying their amplitudes and phase angles. For a plane wave that is arbitrarily polarized the transverse components of the electric field intensity can be written as

$$\begin{aligned} E_x &= a_x \cos(\omega t + \delta_x) \\ E_y &= a_y \cos(\omega t + \delta_y) \end{aligned} \tag{2.5}$$

where a_x and a_y are the amplitudes and δ_x and δ_y are the phase angles along the x- and y-axes respectively. From Eqs. (2.4) and (2.5) the components of d.c. polarization can be written as follows

$$\begin{aligned} p_x &= \frac{\alpha}{2}(a_x^2 - a_y^2) \\ p_y &= -\alpha a_x a_y \cos(\delta_x - \delta_y) \end{aligned} \tag{2.6}$$

Hence the magnitude of d.c. polarization is given by

$$\begin{aligned} |p|^2 &= p_x^2 + p_y^2 \\ &= \frac{\alpha^2}{4}\left[(a_x^4 + a_y^4) + 2a_x^2 a_y^2 \cos 2(\delta_x - \delta_y)\right] \end{aligned} \tag{2.7}$$

For an elliptically polarized wave a_x, a_y and $(\delta_x - \delta_y)$ are arbitrary and therefore the d.c. polarization is given by Eq. (2.7).

For circularly polarized wave

$$a_x = a_y = a \tag{2.8}$$

and

$$\delta_x - \delta_y = \frac{m\pi}{2} \qquad (m = \pm 1, \pm 3, \pm 5, \ldots) \qquad (2.9)$$

Substituting Eqs. (2.8) and (2.9) in Eq. (2.7), one obtains

$$|p| = 0 \qquad (2.10)$$

Thus there exists no d.c. polarization if the propagating wave is circularly polarized.

For a linearly polarized wave a_x and a_y are arbitrary and

$$\delta_x - \delta_y = m\pi \qquad (m = 0, \pm 1, \pm 2, \ldots) \qquad (2.11)$$

Substituting Eq. (2.11) in Eq. (2.7) and taking the square root of both sides, it follows that

$$|p| = \frac{\alpha}{2}(a_x^2 + a_y^2) \qquad (2.12)$$

The direction of the d. c. polarization caused by the linearly polarized wave can be determined by considering Fig. (2.1), where $x'x'$ and $y'y'$ are arbitrary choice of coordinate axes and xx and yy the crystal axes. Without loss of generality it can be assumed that the direction of polarization of the laser beam is along $x'x'$ direction making an angle θ with the x-axis of the crystal. From Eqs. (2.6) and (2.11) it follows that the d.c. polarization along the crystal axes are

$$\begin{aligned} p_x &= \frac{\alpha E_o^2}{2}\cos 2\theta \\ p_y &= \frac{\alpha E_o^2}{2}\sin 2\theta \end{aligned} \qquad (2.13)$$

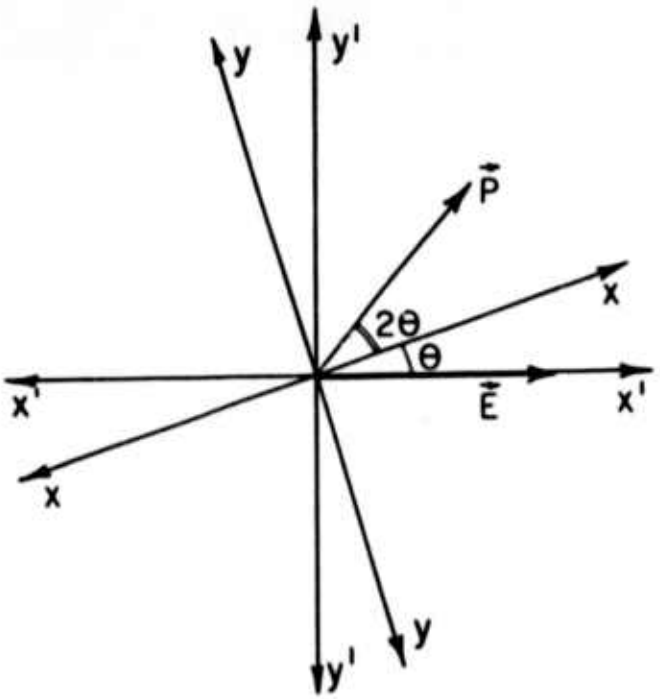

Fig. 2.1. Axes Orientation for Deriving the Angular Dependence of d. c. Polarization for Propagation Along z-axis

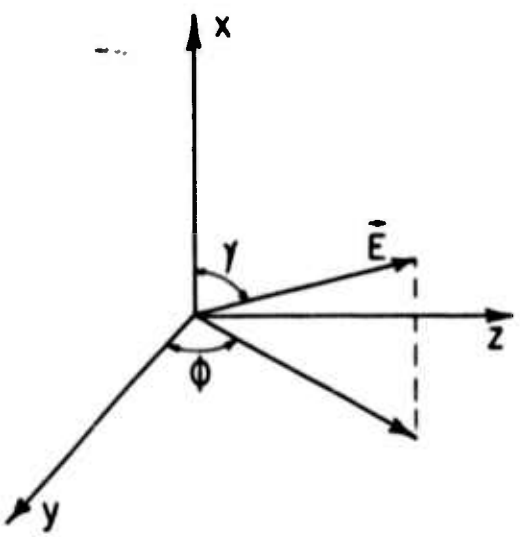

Fig. 2.2. Configuration to Determine the Relationship Between d.c. Polarization and β

where $E_o \cos \omega t$ is the electric field intensity of the incident radiation. From Eqs. (2.13) and Fig. (2.1), it can be seen that if the incident polarization makes an angle θ with the x-axis, the d.c. polarization vector makes an angle -2θ with it. Also from Eqs. (2.13), the magnitude of the d.c. polarization in terms of the electric field intensity of the radiation is given by

$$|p| = \frac{\alpha E_o^2}{2} \tag{2.14}$$

Eqs. (2.12) through (2.14) give the relationship between d.c. polarization and only one of the elements of the second-order nonlinear polarization coefficient tensor. To obtain a similar relationship between the d.c. polarization and the other element β, consider the configuration shown in Fig. (2.2) where x, y, z are the crystal axes. The electric field intensity vector $\vec{E} = \vec{E}_o \cos \omega t$ makes an angle γ with the x-axis and an angle ϕ with the y-axis. Then the components of E along the three axes are

$$\begin{aligned} E_x &= E_o \cos \gamma \\ E_y &= E_o \sin \gamma \cos \phi \\ E_z &= E_o \sin \gamma \sin \phi \end{aligned} \tag{2.15}$$

Here, the frequency dependence has not been explicitly written, but is implied. From Eqs. (2.5) and (2.15) one obtains

$$p_x = \alpha E_o^2 \left[\cos^2 \gamma - \sin^2 \gamma \cos^2 \phi\right] + \frac{\beta E_o^2}{2} \sin^2 \gamma \sin 2\phi \tag{2.16}$$

If the E-vector is made to lie in y-z plane, $\gamma = 90^{\circ}$ and Eq. (2.16) reduces to

$$P_x = \frac{\beta E_o^2}{2} \sin 2\phi - \alpha E_o^2 \cos^2\phi \qquad (2.17)$$

Eq. (2.17) thus yields an expression for the d.c. polarization which is dependent on both the parameters, α and β. Eqs. (2.13) and (2.17) suggest a method of the measurement of the coefficients α and β by measuring the d.c. polarization.

2.2. Angular Dependence of D. C. Polarization for z-axis Propagation

It is evident from Eqs. (2.13) and (2.16) that the direction of d.c. polarization depends on the orientation of the E-vector with respect to the crystal axes. The angular dependence of d.c. polarization for the case of the propagation along z-axis can be determined from Eq. (2.13) and Fig. (2.1). One observes from Eq. (2.13) that with the incident polarization fixed in space, as the crystal is rotated about its z-axis through an angle θ, the d.c. polarization vector is rotated through an angle 2θ in the opposite direction. Thus if the crystal is rotated at the rate of θ, the d.c. polarization will rotate at the rate of 2θ. This is represented in Fig. (2.3).

As mentioned in the introduction, this angular dependence will be one of the important tests in the experimental verification. It will serve to distinguish between the pyroelectric voltage which is developed in a unique direction and the d.c. polarization voltage.

2.3. Energy Considerations

This section deals with the energy and power relationships for an

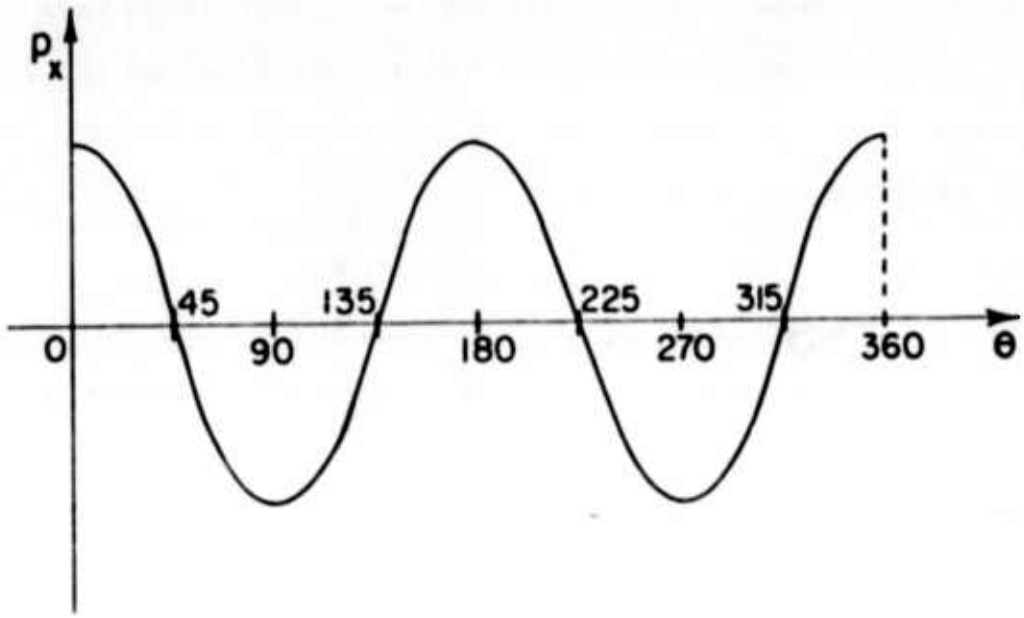

Fig. 2.3. Rotational Dependence of p_x on θ for z-axis Propagation

electromagnetic wave propagating through a nonlinear medium. The procedure followed begins with Maxwell's equations for vacuum and then incorporates the interaction of the wave with the medium by including the distribution of charges and currents. Maxwell's electrodynamic equation for a medium at rest is given by [10]

$$\nabla \times \vec{E} = -\frac{\partial \vec{B}}{\partial t} \tag{2.18}$$

$$\nabla \times \vec{B} = \mu_o(\vec{J}_{true} + \frac{\partial \vec{P}}{\partial t} + \nabla \times \vec{M} + \epsilon_o \frac{\partial \vec{E}}{\partial t}) \tag{2.19}$$

In Eq. (2.19), magnetic induction vector $\vec{B}$ can be replaced by the magnetic intensity vector $\vec{H}$, $\vec{B} = \mu_o \vec{H}$, and $\vec{M}$ may be set equal to zero, since only non-magnetic media are of interest in the present work. It is further assumed that the dielectric medium is lossless which reduces Eqs. (2.18) and (2.19) to

$$\nabla \times \vec{E} = -\mu_o \frac{\partial \vec{H}}{\partial t} \tag{2.20}$$

$$\nabla \times \vec{H} = \frac{\partial}{\partial t}\left[\epsilon_o \vec{E} + \vec{P}\right] \tag{2.21}$$

It is worth mentioning here that nonlinearity is implicit in Eq. (2.21) since $\vec{P}$ is comprised of linear as well as nonlinear polarization terms as expressed by Eq. (1.3). Taking the scalar product of Eq. (2.20) with $\vec{H}$ and Eq. (2.21) with $\vec{E}$ and subtracting the latter from the former, one obtains

$$\nabla \cdot \vec{s} + \mu_o \vec{H} \cdot \frac{\partial \vec{H}}{\partial t} + \epsilon_o \vec{E} \cdot \frac{\partial \vec{E}}{\partial t} + \vec{E} \cdot \frac{\partial \vec{P}}{\partial t} = 0 \tag{2.22}$$

where $\vec{s} = \vec{E} \times \vec{H}$ is the Poynting vector. Eq. (2.22) is the well known

energy balance equation of the system. To put it in a more familiar form, we define the energy density per unit volume in the medium as U. Then

$$\frac{\partial U}{\partial t} = \vec{E} \cdot \frac{\partial \vec{P}}{\partial t} \tag{2.23}$$

Eq. (2.22) can now be written as

$$\nabla \cdot \vec{S} + \mu_o \vec{H} \cdot \frac{\partial \vec{H}}{\partial t} + \epsilon_o \vec{E} \cdot \frac{\partial \vec{E}}{\partial t} + \frac{\partial U}{\partial t} = 0 \tag{2.24}$$

Eq. (2.24) shows that the power flow out of the medium is equal to the rate at which the stored energy in the electromagnetic field is decreasing $[(-\mu_o \vec{H} \cdot \partial\vec{H}/dt) - (\epsilon_o \vec{E} \cdot \partial\vec{E}/dt)]$ plus the rate at which the material is doing work on the electromagnetic field $[-\partial U/\partial t]$.

Restricting our attention to the d.c. part produced by the second-order nonlinear term, it is obvious from Eq. (2.23) that there is no net transfer of energy from the wave under steady state conditions. This does not mean, however, that there is no energy transfer when the field is turned on. In fact, the wave does work on the system to establish the d.c. field. It will be shown in Section 3.2 that part of this work will be extracted from the system if there is an external mechanism present in the region of the field.

Chapter 3

DETECTING TECHNIQUE AND CIRCUIT CONSIDERATIONS

This chapter is devoted to description of the detection technique and the circuit considerations that play a part in it. In order to facilitate an understanding of the basic interaction phenomena between the field set up by the electromagnetic wave and the external detecting circuitry, a simple model is chosen and an analysis of it is made. An equivalent circuit is derived for use in the later chapters. It is shown that no d.c. power can be extracted from the system (i.e., there exists no optical power rectification). However, the system has the capability of detecting low frequency modulation.

3.1. Interaction Between Electromagnetic Wave and Detecting Circuitry

The nonlinear polarization can be detected with the use of an external circuit arrangement of the type described below. The medium in which the nonlinear polarization is established is made part of a capacitor that is formed by two electrodes that are placed on opposite sides of the dielectric. The capacitor thus formed is then connected to an external detector. The arrangement shown in Fig. (3.1) represents the simple case of a parallel plate capacitor formed with the nonlinear dielectric medium.

To find the voltage across the capacitor, the potential problem

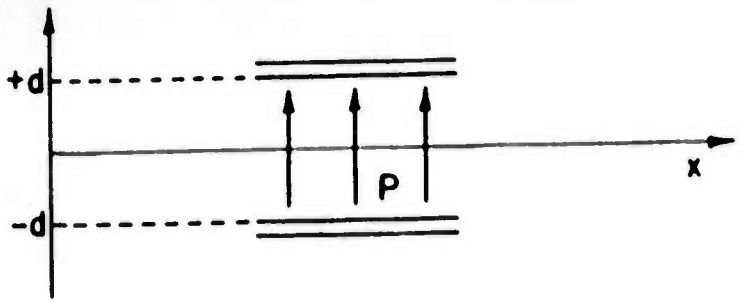

Fig. 3.1. Detector Model Assumed in Section 3.1

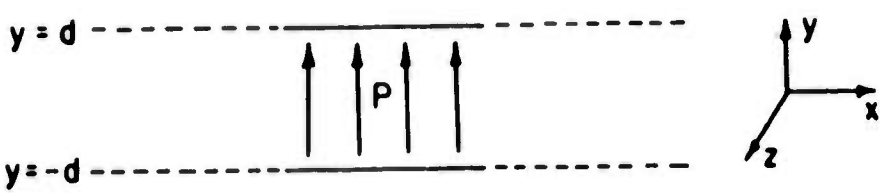

Fig. 3.2. Configuration for Potential Described by Eqs. (3.1) and (3.2)

considered in Fig. (3.2) is first solved. Here the dielectric medium is considered infinite along the x and z-directions and of breadth 2d in the y-direction. The general solution for potential satisfying the Laplace's equation can be written as

$$V_1 = A_o + A_1 y \tag{3.1}$$

$$V_2 = B_o + B_1 y \tag{3.2}$$

where V_1 is the potential inside the dielectric and V_2 the potential outside the dielectric. From symmetry considerations $A_o = 0$ and $B_1 = 0$. Hence Eq. (3.1) and (3.2) reduce to

$$V_1 = A_1 y \tag{3.3}$$

$$V_2 = B_o \tag{3.4}$$

The two unknown constants in Eqs. (3.3) and (3.4) can be solved by specifying the two boundary conditions. Equating the potential at $y = d$, one obtains

$$A_1 d = B_o \tag{3.5}$$

The second boundary condition involves the discontinuity in the normal displacement vector. Since no true charge has physically been introduced into the system, one has from Maxwell's equation

$$\nabla \cdot \vec{D} = 0 \tag{3.6}$$

However, the displacement vector includes two kinds of polarizations, the internal polarization $\vec{P}_i$ caused by the material property and the ex-

ternal polarization $\vec{P}_e$ that is induced into the system by an external agency (in the present case the nonlinear field). Thus $\vec{D}$ can be written as

$$\vec{D} = \epsilon_o \vec{E} + \vec{P}_i + \vec{P}_e \tag{3.7}$$

where ϵ_o is the permittivity of free space. Substituting Eq. (3.7) in Eq. (3.6), one has

$$\nabla \cdot (\epsilon_o \vec{E} + \vec{P}_i) = - \vec{P}_e \tag{3.8}$$

Let

$$- \nabla \cdot \vec{P}_e = \rho_P \tag{3.9}$$

where ρ_P is the polarization charge density. From Eqs. (3.8) and (3.9), it is seen that

$$\nabla \cdot (\epsilon_o \vec{E} + \vec{P}_e) = \rho_P \tag{3.10}$$

Thus it is observed that even though only polarization charges are involved, the external polarization charge behaves as a true charge for the system under consideration. Since the polarization is assumed to be uniform in Fig. (3.2), $\nabla \cdot \vec{P} = 0$ everywhere except on the boundary. The second boundary condition at y = d is therefore

$$- \epsilon_o \frac{\partial V_2}{\partial y} + \epsilon \frac{\partial V_1}{\partial y} = P_e \tag{3.11}$$

where ϵ is the permittivity of the dielectric at low frequencies. From

Eqs. (3.3), (3.4), and (3.11), one has

$$A_1 = \frac{P_e}{\epsilon} \tag{3.12}$$

Substituting Eq. (3.12) in (3.3), and letting y = d

$$V_1 = \frac{P_e d}{\epsilon} \tag{3.13}$$

This result can be applied to the case shown in Fig. (3.1) without any fringe effects. The voltage across the capacitor is then given by

$$V_Q = \frac{2P_e d}{\epsilon} \tag{3.14}$$

Now, consider the circuit shown in Fig. (3.3) where the capacitor is connected to an external detector with an input capacitance C and an input resistance R. The nodal equation at the node A is

$$\frac{dQ}{dt} + \frac{V_o}{R} + C\frac{dV_o}{dt} = 0 \tag{3.15}$$

where V_o is the instantaneous voltage across the capacitor plates and Q is the charge on them. The charge Q on the plate is due to the external polarization source plus the depolarizing effect in the material. Assuming unit area for the capacitor plates, the total charge on the capacitor is

$$Q = \epsilon E + P_e \tag{3.16}$$

Substituting Eq. (3.16) in Eq. (3.15), one has

$$\frac{dV_o}{dt}\left(\frac{\epsilon}{2d} + C\right) + \frac{V_o}{R} + \frac{dP_e}{dt} = 0 \quad . \tag{3.17}$$

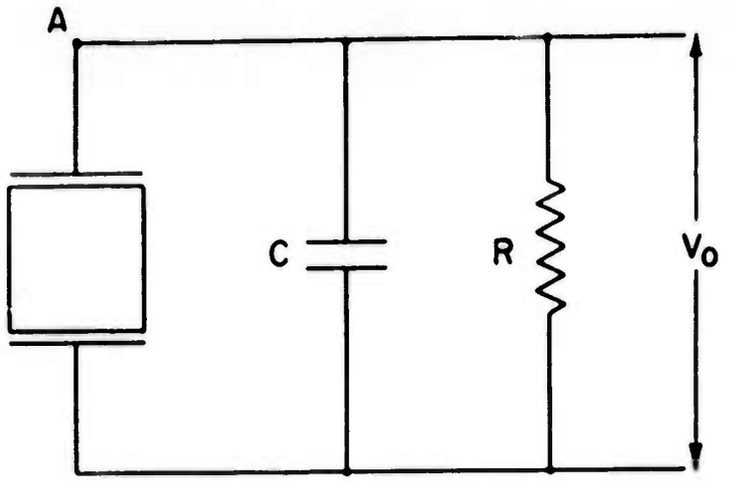

Fig. 3.3. The Quartz Detector with External Circuitry

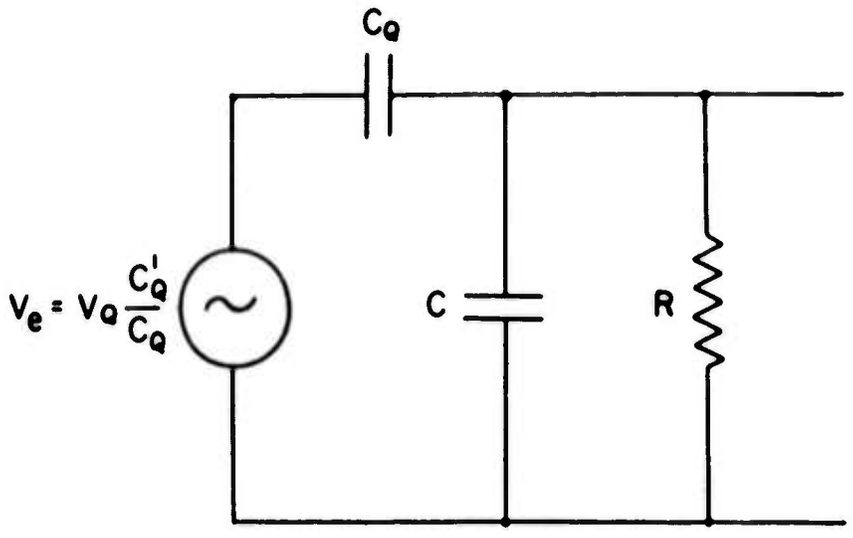

Fig. 3.4. Equivalent Circuit for the Configuration of Fig. 3.3

where E has been replaced by $V_o/2d$. For the non-fringing case that is under consideration, $\epsilon/2d$ is the capacitance of the capacitor formed with the nonlinear dielectric. If this capacitance is designated by C_Q, then Eq. (3.17) can be rewritten as

$$\frac{dV_o}{dt} + \frac{V_o}{(C_Q + C)R} + \frac{1}{(C_Q + C)} \frac{dP_e}{dt} = 0 \tag{3.18}$$

Taking the Laplace transform of Eq. (3.18) and letting the initial conditions be zero, one has

$$V_o(s) = - \frac{P_e(s)}{C_Q + C} \frac{s}{s + \frac{1}{(C_Q + C)R}} \tag{3.19}$$

But, from Eq. (3.14) one has

$$P_e(t) = V_Q(t)\, C_Q' \tag{3.20}$$

where C_Q' is an equivalent capacitance which is explained later in this section and is given by

$$C_Q' = \frac{\epsilon}{2d} = C_Q \tag{3.21}$$

Hence

$$P_e(s) = V_Q(s)\, C_Q$$

Substituting the value of $P_e(s)$ in Eq. (3.19), one obtains

$$V_o(s) = - \frac{V_Q(s)\, C_Q}{C_Q + C} \frac{s}{s + \frac{1}{(C_Q + C)R}} \tag{3.22}$$

In Eq. (3.21), a distinction has been made between C_Q and C_Q' although these two quantities are equal in the present simple case. If, however, there is an air gap between each plate and the dielectric, then C_Q and C_Q' will be different. C_Q is the actual capacitance of the system whereas C_Q' is an equivalent capacitance formed with the dielectric alone present. Thus the general expression for the output voltage is written by modifying Eq. (3.22).

$$V_o(s) = - \frac{V_Q(s)\, C_Q'}{C_Q + C} \frac{\frac{s}{1}}{s + (C_Q + C)R} \tag{3.23}$$

Rewriting Eq. (3.23)

$$V_o(s) = - \frac{V_e(s)\, C_Q}{C_Q + C} \frac{\frac{s}{1}}{s + (C_Q + C)R} \tag{3.24}$$

where

$$V_e = V_Q \frac{C_Q'}{C_Q} \tag{3.25}$$

Eq. (3.24) describes the circuit which is shown in Fig. (3.4), and Fig. (3.4) thus shows the equivalent circuit model for the configuration shown in Fig. (3.3).

3.2. Output Response for a Continuous Laser Beam Propagating Through the Medium

Consider the case of a continuous laser beam that is turned on to time t = 0. After time t = 0 the beam traverses the medium continuously in time with the same intensity. The polarization in the medium can

thus be represented by a step function $P_e = P_o\, u(t)$ as shown in Fig. (3.5a). For such a driving function the output response $V_o(t)$ is given by

$$V_o(t) = -\frac{V_e C_Q}{C_Q + C} e^{-t/(C_Q+C)R} \tag{3.26}$$

The response given by Eq. (3.26) is shown in Fig. (3.5b). It can be seen that there is no average d.c. output. Thus if a continuous laser beam of constant intensity traverses the medium, the d.c. polarization set up under these conditions does not yield any power output except during the transient condition. This is in accordance with the conclusion arrived at from the field theory approach in Section 2.3.

3.3. Low-Frequency Intensity Modulation Detector

The technique of detection outlined above can be used as a modulation detector in the case of laser pulse having low frequency modulation. This is of practical interest since the actual ruby laser output is comprised of spikes that occur once in a microsecond.

For the purpose of analysis, if one consider the external polarization to vary sinusoidally, then

$$P_e(t) = P_o \cos \omega t \tag{3.27}$$

Then

$$P_e(s) = \frac{P_o s}{s^2 + \omega^2} \tag{3.28}$$

From Eqs. (3.20), (3.24), (3.25) and (3.28) it follows that

$$V_o(s) = -\frac{P_o R}{\omega^2} \frac{s^2}{(1 + \frac{s^2}{\omega^2})(1 + \tau s)} \tag{3.29}$$

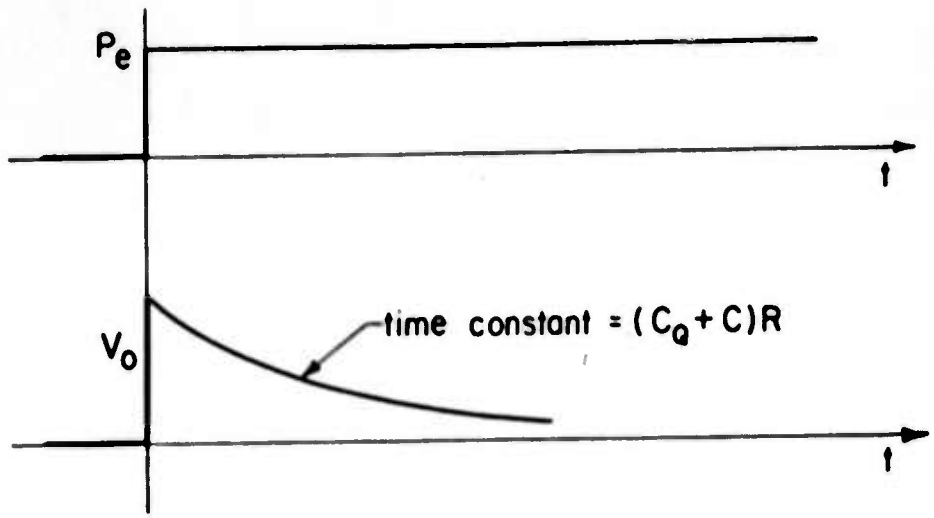

Fig. 3.5. Output Response to a Continuous Laser Beam Travelling Through the Nonlinear Medium

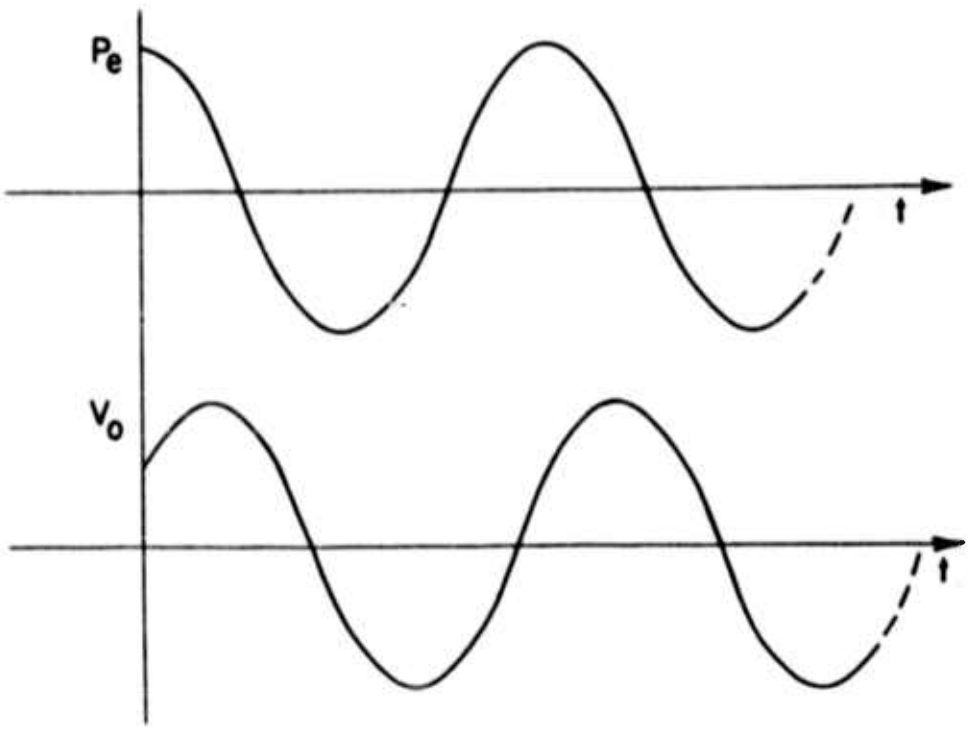

Fig. 3.6. Output Response to a Sinusoidally Intensity Modulated Beam Travelling Through the Nonlinear Medium

where

$$\tau = \frac{1}{(C_Q + C)R} \tag{3.30}$$

Taking the inverse transform

$$V_o(t) = \frac{P_o R}{\omega^2}\left[\frac{\omega^2}{\tau(1 + \tau^2\omega^2)} e^{-t/\tau} - \frac{\omega^3 \sin(\omega t - \psi)}{(1 + \tau^2\omega^2)^{1/2}}\right] \tag{3.31}$$

where

$$\psi = \tan^{-1} \omega\tau \tag{3.32}$$

Under steady state condition, Eq. (3.31) reduces to

$$V(t) = \frac{P_o R \omega}{(1 + \tau^2\omega^2)^{1/2}} \sin(\omega t - \psi) \tag{3.33}$$

Eq. (3.33) shows that there is an output at the same frequency as the modulation, thus proving that system could be used as an intensity modulation detector. Fig. (3.6) represents this case.

The above result is of practical importance in establishing the relationship between the shape of the laser pulse and the shape of the d. c. polarization pulse. The actual ruby laser output is comprised of a series spikes that occur at the rate of once a microsecond as shown in Fig. (3.7a). The d. c. polarization should theoretically exhibit this spiking phenomena as represented in Fig. (3.7b). However, as will be explained in Chapter 5, there may be measurement difficulty in observing this phenomenon if the laser power output is low.

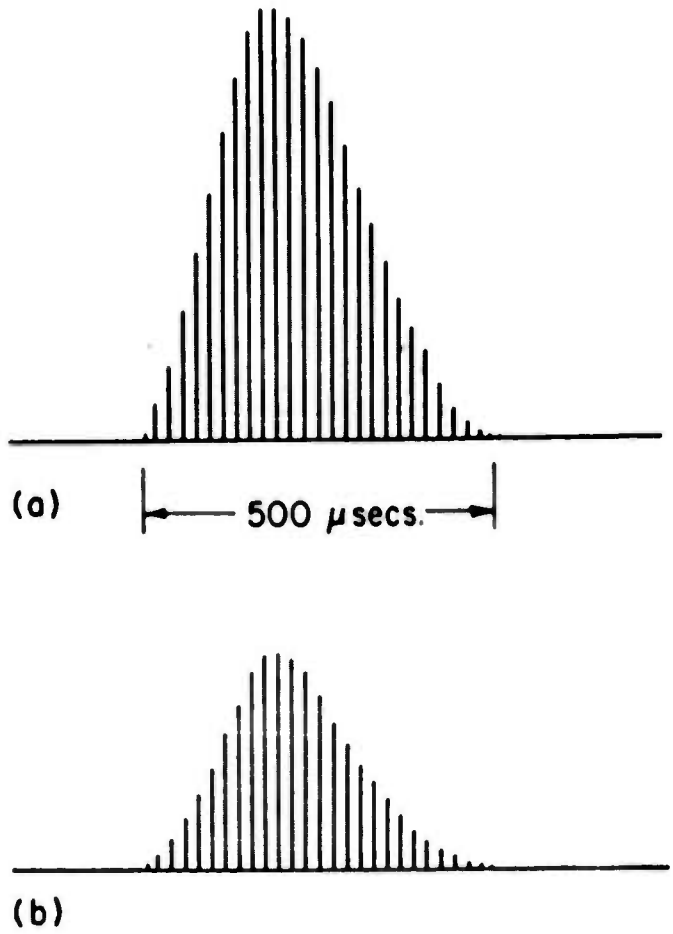

Fig. 3.7. Output Response to an Actual Laser Pulse

(a) Laser Output as a series of spikes

(b) d.c. polarization caused by (a)

Chapter 4

APPLICATION OF THE PHENOMENON OF D. C. POLARIZATION TO LASER POWER MEASUREMENT

In this chapter a new method of measuring power in a high power laser pulse is proposed. The method makes use of the d. c. polarization that is developed when a high intensity laser beam traverses through a medium like quartz. It is shown that the d. c. polarization is directly proportional to the intensity in the laser beam.

4.1. A Boundary Value Problem

Consider a circular cylindrical quartz crystal rod with the optic axis oriented along the length of the rod. Let the laser beam propagate along the axial direction. Fig. 4.1 shows the cross-section of the cylindrical quartz rod of radius b with its z-axis perpendicular to the plane of the paper. The incident laser beam is assumed to be linearly polarized and cylindrical in cross-section. The radius of the beam is a.

Let the laser beam cause a uniform d. c. polarization given by Eq. (2.14) in the transverse direction making an angle ϕ with the x-axis of the crystal. Since quartz is a uniaxial crystal, the x-y plane is isotropic. Let the permittivity in the transverse direction at low frequencies be ϵ. This can be considered as a two-dimensional electrostatic problem for the case of the crystal of infinite length.

Due to the cylindrical symmetry of the problem, the solution for

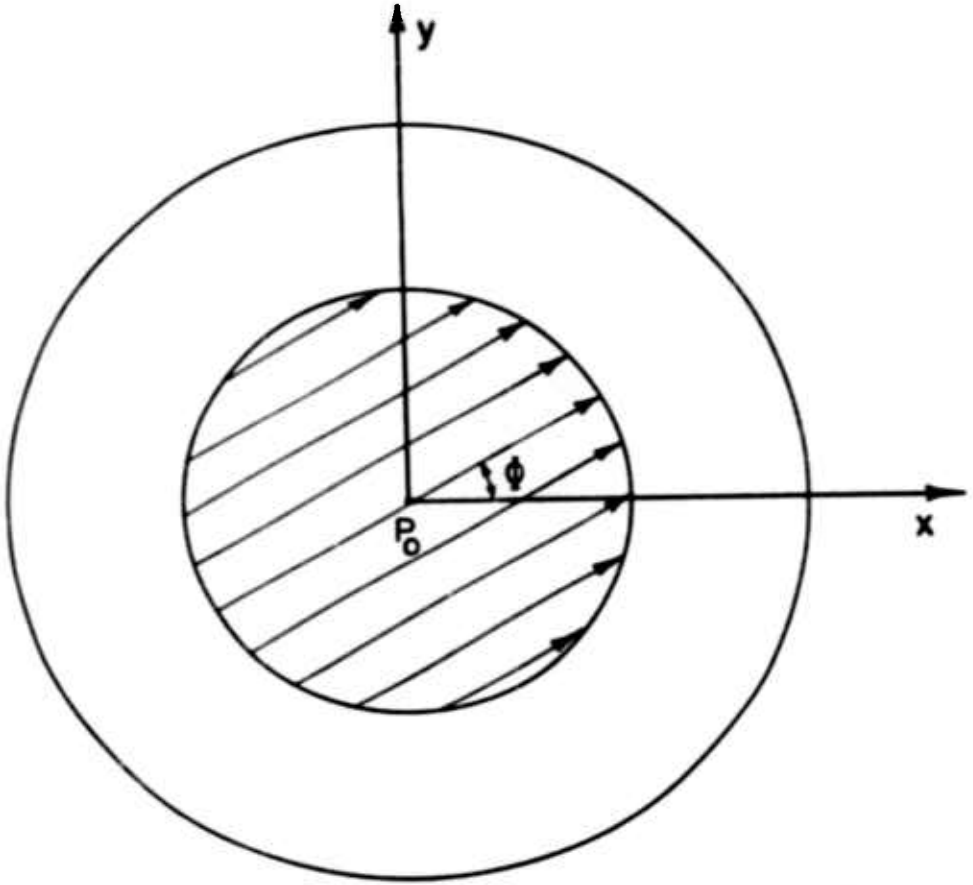

Fig. 4.1. Cross-Section of the Quartz Rod with Concentric Laser Beam

the potential may be expanded in terms of cylindrical harmonics. The potentials in the three regions thus take on the forms,

$$V_1 = \sum_{n=1}^{\infty} A_n r^n \cos n(\theta - \phi) \tag{4.1}$$

$$V_2 = \sum_{n=1}^{\infty} (B_n r^n + C_n r^{-n}) \cos n(\theta - \phi) \tag{4.2}$$

$$V_3 = \sum_{n=1}^{\infty} D_n r^{-n} \cos n(\theta - \phi) \tag{4.3}$$

Here V_1 represents the potential in the region of crystal filled by the laser beam, V_2 the potential in the region of the crystal not filled by the laser beam and V_3 the potential outside the crystal medium. A_n, B_n, C_n and D_n are constants that are to be determined, and θ is the angle measured from the x-axis. The d. c. polarization P_o makes an angle ϕ with the positive x-axis.

For the uniform dipole polarization P_o, all constants A_n, B_n, C_n and D_n are zero except for $n = 1$. Thus, Eqs. (4.1) to (4.3) reduce to

$$V_1 = A_1 r \cos(\theta - \phi) \tag{4.4}$$

$$V_2 = (B_1 r + C_1 r^{-1}) \cos(\theta - \phi) \tag{4.5}$$

$$V_3 = D_1 r^{-1} \cos(\theta - \phi) \tag{4.6}$$

Eqs. (4.4) to (4.6) have four unknown constants which can be determined by making use of the two boundary conditions at $r = a$ and the two boundary conditions at $r = b$, where a and b are the radii of the

laser beam and the crystal respectively and a < b.

As mentioned in Section 3.1, care must be exercised in describing the boundary conditions at r = a. A clear distinction has to be made between the external polarizing source and the internal depolarizing field of the medium.

$$\vec{D} = \epsilon_o \vec{E} + \vec{P}_1 + \vec{P}_o \tag{4.7}$$

Since there are no true charges introduced into the system,

$$\nabla \cdot \vec{D} = 0 \tag{4.8}$$

Substituting Eq. (4.7) in Eq. (4.8),

$$\nabla \cdot (\epsilon_o \vec{E} + \vec{P}_1 + \vec{P}_o) = 0$$

or

$$\nabla \cdot \epsilon \vec{E} = - \nabla \cdot \vec{P}_o \tag{4.9}$$

Inside the circle r < a, P_o is uniform and hence the right hand side of Eq. (4.9) is zero. However at the boundary r = a

$$- \nabla \cdot \vec{P}_o = \vec{P}_o \cdot \vec{n} \tag{4.10}$$

where $\vec{n}$ is the unit vector normal to the surface at r = a. Thus the boundary conditions at r = a are

$$\epsilon \frac{\partial V_1}{\partial r} - \epsilon \frac{\partial V_2}{\partial r} = P_o \cos(\theta - \phi) \tag{4.11}$$

$$V_1 = V_2 \tag{4.12}$$

At r = b

$$\epsilon \frac{\partial V_2}{\partial r} - \epsilon_o \frac{\partial V_3}{\partial r} = 0 \tag{4.13}$$

$$V_2 = V_3 \tag{4.14}$$

In the above equations ϵ_o is the free space permittivity, ϵ_r the dielectric constant of the crystal in the transverse plane and $\epsilon = \epsilon_o \epsilon_r$.

Making use of Eqs. (4.11) to (4.14) in Eqs. (4.4) to (4.6), one obtains the following equations for the constants.

$$A_1 = \frac{a^2 P_o (\epsilon_r - 1)}{2\epsilon b^2 (\epsilon_r + 1)} + \frac{P_o}{2\epsilon} \tag{4.15}$$

$$B_1 = \frac{a^2 P_o}{2\epsilon b^2} \frac{(\epsilon_r - 1)}{(\epsilon_r + 1)} \tag{4.16}$$

$$C_1 = \frac{a^2 P_o}{2\epsilon} \tag{4.17}$$

$$D_1 = \frac{a^2 P_o}{\epsilon_o (\epsilon_r + 1)} \tag{4.18}$$

Substituting Eqs. (4.15) to (4.18) in Eqs. (4.4) to (4.6), the following potential solutions for the boundary value problem are obtained.

$$V_1 = \left[\frac{a^2 P_o (\epsilon_r - 1)}{2\epsilon b^2 (\epsilon_r + 1)} + \frac{P_o}{2\epsilon} \right] r \cos(\theta - \phi) \tag{4.19}$$

$$V_2 = \left[\frac{a^2 P_o (\epsilon_r - 1)}{2\epsilon b^2 (\epsilon_r + 1)} r + \frac{a^2 P_o}{2\epsilon} \frac{1}{r} \right] \cos(\theta - \phi) \tag{4.20}$$

$$V_3 = \frac{a^2 P_o}{\epsilon_o (\epsilon_r + 1)} \frac{1}{r} \cos(\theta - \phi) \tag{4.21}$$

4.2. An Ideal Power Meter

From Eq. (4.21) the voltages on the boundary of the crystal along the two axes are given by

$$V_x = \frac{2P_o a^2}{\epsilon_o (\epsilon_r + 1) b} \cos \phi \tag{4.22}$$

$$V_y = \frac{2P_o a^2}{\epsilon_o (\epsilon_r + 1) b} \sin \phi \tag{4.23}$$

Note that $V_x = 2V_{3x}$ and $V_y = 2V_{3y}$.

If the power in the laser beam is P_L, then the electric field intensity $E = E_o \cos \omega t$ is given by

$$E_o^2 = \frac{2\eta}{\pi a^2} P_L \tag{4.24}$$

where η is the intrinsic impedance of the crystal medium in the transverse direction. In deriving Eq. (4.24) the laser beam is assumed to be propagating in an infinite medium. Substituting Eq. (4.24) in Eq. (2.14), one has

$$P_o = \frac{\alpha\eta}{\pi a^2} P_L \tag{4.25}$$

From Eqs. (4.22), (4.23) and (4.25)

$$V_x = K P_L \cos \phi \tag{4.26}$$

$$V_y = K P_L \sin \phi \tag{4.27}$$

where

$$K = \frac{2\alpha\eta}{\pi b \epsilon_o(\epsilon_r + 1)} \tag{4.28}$$

Eqs. (4.26) and (4.27) express the d. c. polarization in terms of the power content in the laser beam. Adding these two voltages in quadrature, the following relationship between the net d. c. polarization and the power in the laser beam is obtained.

$$V = K P_L \tag{4.29}$$

where

$$V = (V_x^2 + V_y^2)^{1/2} \tag{4.30}$$

The following interesting observations can be made from Eq. (4.29):

1) The voltage is linearly proportional to the power in the laser beam.
2) The voltage is dependent only on the power in the laser beam and not on the size of the laser beam, as long as the entire beam is contained within the crystal. Thus any focusing or defocusing effect of the beam does not affect the voltage V.
3) It is also easy to observe the fact that even though the

above equation has been derived assuming that the power density in the laser beam is uniform, the result will hold true even for the case where the power density in the beam is only a function of the radius.

These important features make this principle attractive for measuring the power in the laser beam.

4.3. Device Considerations

The basic principle of the power meter was described in the previous section. A practical method of applying this principle will now be presented. Consider again the configuration of the z-cut quartz shown in Fig. (4.1). The laser beam propagates along the z-axis and is concentric with the cylinder. From Eqs. (4.21) and (4.25) one obtains the following equation describing the potential outside the cylinder in terms of the power in the laser beam.

$$V = \frac{\alpha\eta}{\pi \epsilon_o(\epsilon_r + 1)} P_L \frac{1}{r} \cos(\theta - \phi) \qquad (4.31)$$

The equipotential lines described by Eq. (4.31) with $\phi = 0$, are shown in Fig. (4.2). It can be observed that the equation $r = k \cos\theta$, where k is an arbitrary constant, describes equipotential surfaces.

Substituting $r = k \cos\theta$ in Eq. (4.31), one obtains

$$V = K_1 P_L \qquad (4.32)$$

where

$$K_1 = \frac{\alpha\eta}{k\pi \epsilon_o(\epsilon_r + 1)} \qquad (4.33)$$

For various values of k, Eq. (4.32) describes equipotential sur-

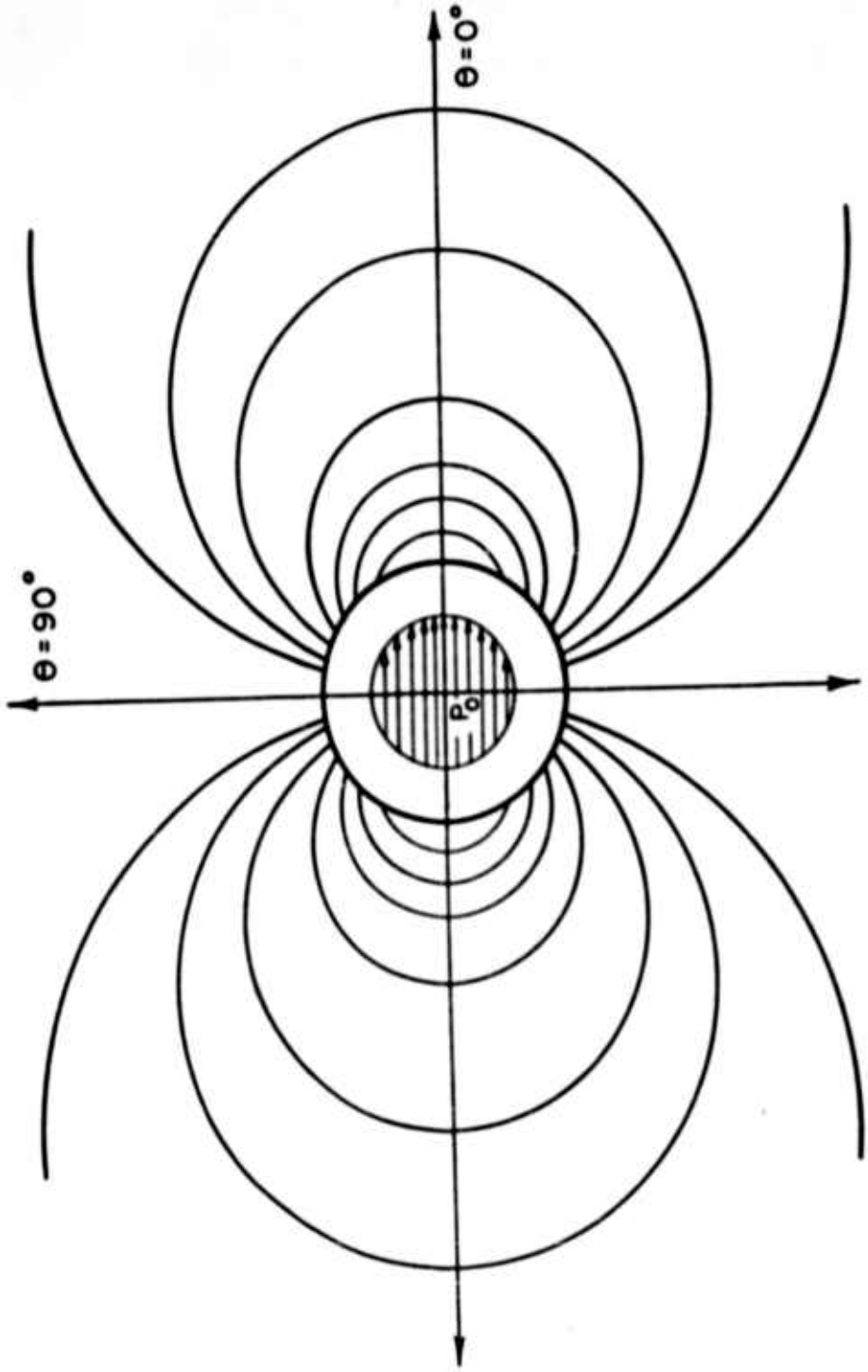

Fig. 4.2. Equipotential Lines Outside the Quartz Medium

faces outside the quartz crystal which are pairs of circles with centers at $(\pm k K_1 P_L/2, 0)$ and of radius of $k K_1 P_L/2$.

For the actual construction of the power meter, a pair of electrodes is placed along these equipotential lines $\pm V$ corresponding to $r = k_1 \cos\theta$. The plates are aligned perpendicular to the x-axis of the crystal. The two plates form a capacitance with voltages $+V$ and $-V$ on the two plates. For the purpose of analysis it is now assumed that the laser beam is linearly polarized along the x-axis of the crystal. (For a laser beam that is not linearly polarized, power measurement could be made by separating it into spatially orthogonal components and making individual measurement of each). From Eq. (4.29) the voltage across the plates is given by

$$V_Q = K_2 P_L \tag{4.34}$$

where

$$K_2 = \frac{2m}{k_1 \pi \epsilon_o (\epsilon_r + 1)} \tag{4.35}$$

The equivalent circuit for the system was derived in Section 3.1 and is shown in Fig. (4.3). In the equivalent circuit C_Q represents the capacitance formed by the two electrodes, C the input capacitance and R the input resistance of the measuring device. The maximum output voltage according to Eq. (3.28) is given by

$$V_{o_{max}} = \frac{V_e C_Q}{C + C_Q} = \frac{K_2 C_Q'}{C + C_Q} P_L \tag{4.36}$$

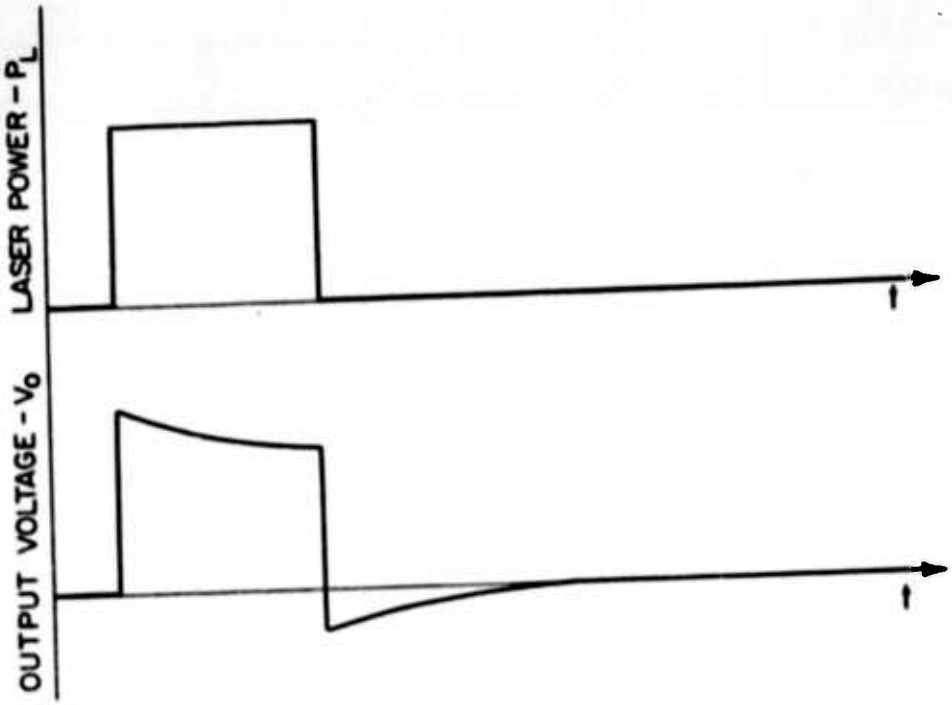

Fig. 4.4. Output Response to a Square Laser Pulse

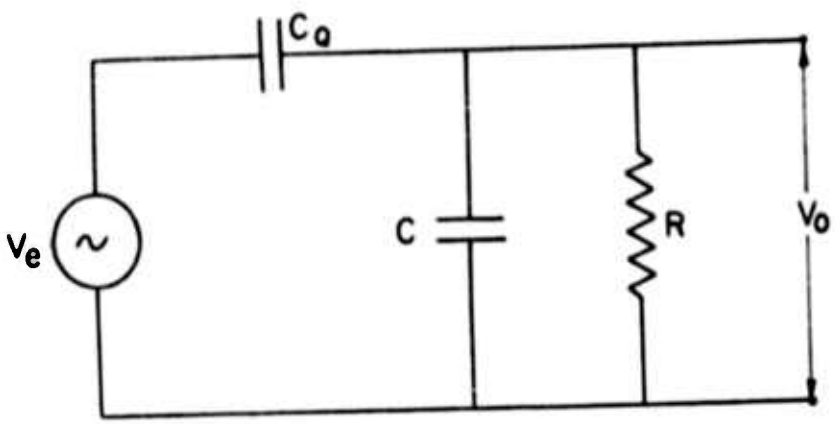

Fig. 4.3. Equivalent Circuit Model of the Quartz Detector

4.4. Discussion

It is seen from Eq. (4.36) that to obtain large output voltage, the input capacitance has to be made as small as possible. An idealized rectangular laser pulse and the response of the circuit for such a pulse are shown in Fig. (4.4). The output voltage follows the laser pulse faithfully if the time constant of the circuit is large compared to the duration of the pulse.

The output voltage V_o directly measures the laser power at any instant. The total energy in the laser pulse can be determined by integrating the output over the period of duration of the pulse.

Chapter 5

EXPERIMENTS AND RESULTS

Theoretical results on many aspects of the phenomenon of nonlinear d. c. polarization in crystals were derived in the preceding chapters. Experimental verification using quartz crystal for some of them is presented in this chapter. It was not possible to verify all the theoretical results due to the lack of availability of a laser that delivered high enough power output.

5.1. Quartz Detector Mount

The theory on detecting technique was presented in Chapter 3. Chapter 4, though has been devoted toward the theory on the application of the phenomenon of d. c. polarization for power measurement, suggests a method for practical construction of a detector. Any detector that is constructed for verifying the theoretical results mentioned in the earlier chapters should satisfy the following requirements.

1) The crystal holder that supports the sample should exert no strain on it.
2) The field set up by the d. c. polarization in the crystal should be undisturbed by the detecting system.
3) The level of the d. c. signal being small, external noise pick-ups and the noise figure of the detecting circuitry should be reduced to a minimum.
4) The crystal mount should have facility to be rotated about its axis.

5) The impedance of the crystal holder being high, the external detecting system should also be designed for high input impedance.

A special mount for the quartz was made that satisfied the above requirements. The mount is an assembly of the crystal holder, rotating mechanism and the built-in preamplifier. A perspective picture of this is shown in Fig. (5.1). A metallic cylinder encloses a plastic crystal holder with electrodes and the preamplifier. The preamplifier, the details of which are described in the following section, is mounted on the rear side of the cylinder. The metal cylinder is supported at the ends by two flanges mounted on a common base such that it can be rotated about its axis. The holes on the front and rear end of the cylinder permit the laser beam to travel through the crystal and out without any obstruction.

A cut-away view of the crystal holder and electrode assembly is shown in Fig. (5.2). This part of the assembly is made with insulator material to minimize any disturbance of the potential field configuration set up by the d.c. polarization. Two flanges with circular holes at the center keep the cylindrical crystal in position and do not interfere with the path of the laser beam. It was shown in Section 4.4 that the equipotential surfaces outside the quartz medium are described by the equation $r = k \cos \theta$, where k is a constant. A pair of electrodes suitably shaped is placed along a pair of these equipotential surfaces $r = k_1 \cos \theta$. It is seen from Fig. (4.2) that highest potential surfaces are closest to the quartz cylinder. Thus to obtain a large output voltage across the electrodes the plates should be close to the quartz cylinder. However

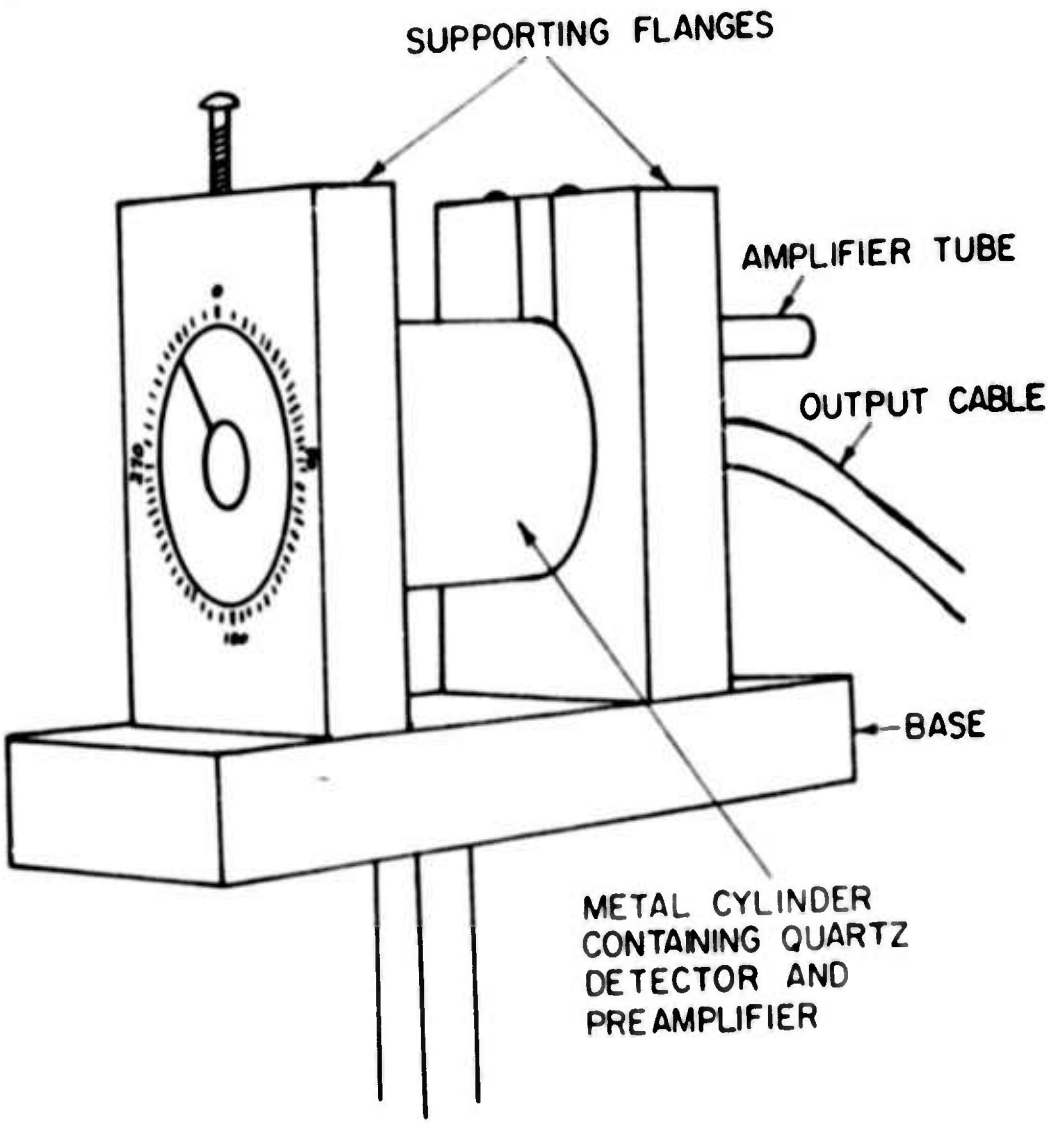

Fig. 5.1. Perspective View of the Crystal Mount

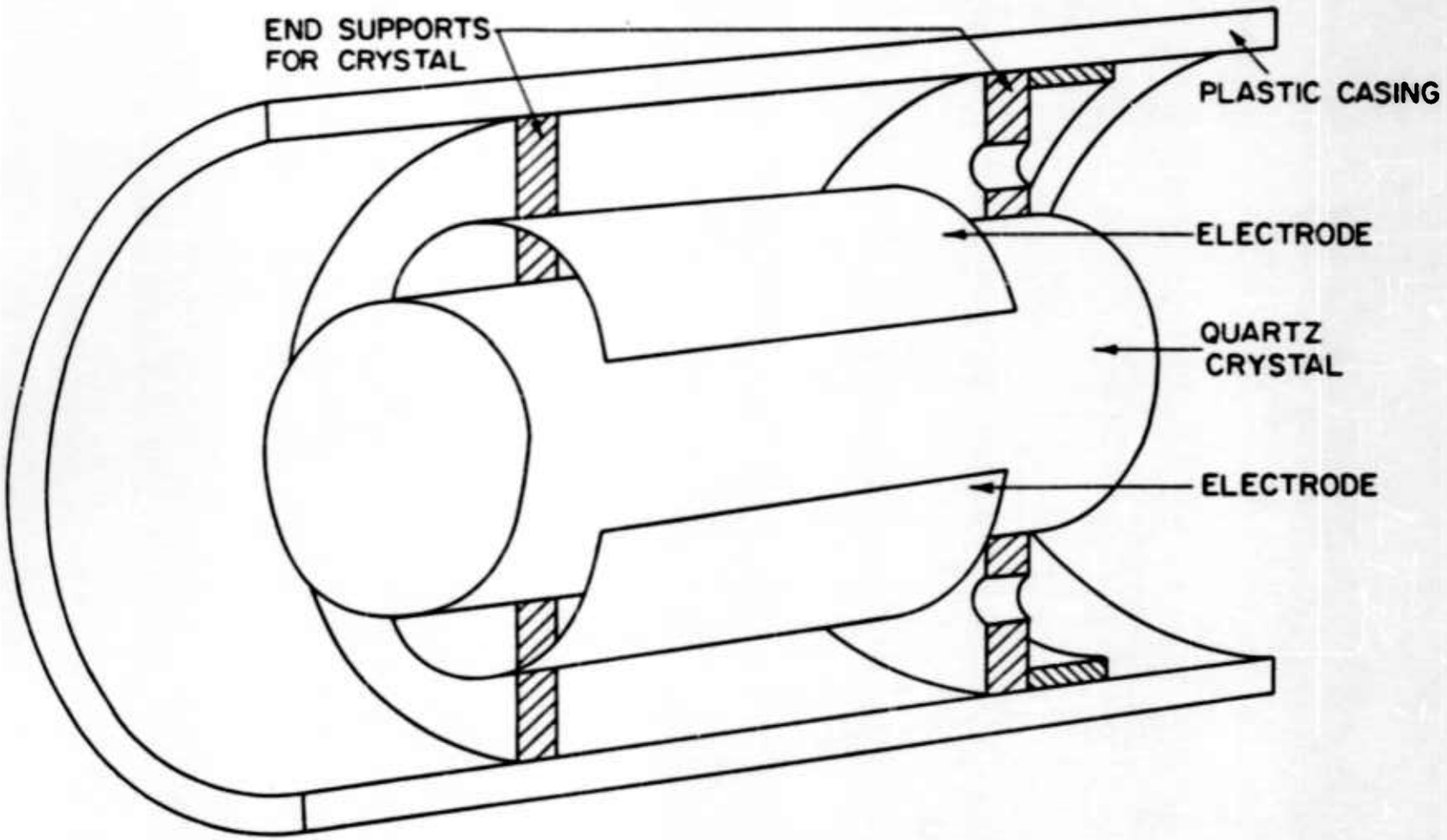

Fig. 5.2. Cut-Away View of Quartz Detector

to obtain a large output voltage V_o in Fig. (4.3) C_Q should be large which means that the value of the capacitance formed by the electrodes should be large. This necessitates as large an area as possible for the electrodes. Thus the two factors oppose each other in choosing the constant k_1 and a compromise has to be made for optimum design.

The orientation of the crystal with respect to the electrodes should be such that it would establish the d.c. polarization in a direction that would cause an equipotential surface along the orientation of the electrodes. For a z-cut quartz crystal, i.e., propagation along the optic axis, if the linearly polarized electromagnetic wave is made to coincide along the x-axis, then the d.c. polarization is also along x-axis. For such a case the plates are aligned perpendicular to the x-axis of the crystal. A side view of the beam, orientation of the crystal and the plates is shown in Fig. (5.3).

5.2. Preamplifier Circuit

The primary requirements of the preamplifier are that it should have a high input impedance and low noise figure. It was pointed out in Section 3.5 that to obtain a large output signal, the input capacitance of the amplifier should be as small as possible. This immediately suggests the use of a cathode follower. To reduce the external noise pick-ups a balanced cathode follower is used, a circuit diagram of which is shown in Fig. (5.4). The circuit uses a subminiature tube CK 6112 which is a twin triode. The choice of this tube was made from considerations of size and the input capacitance. The filament supply is obtained from a d.c. source to keep down the noise figure of the amplifier. The plate supply voltage is 125 volts and the bias voltage

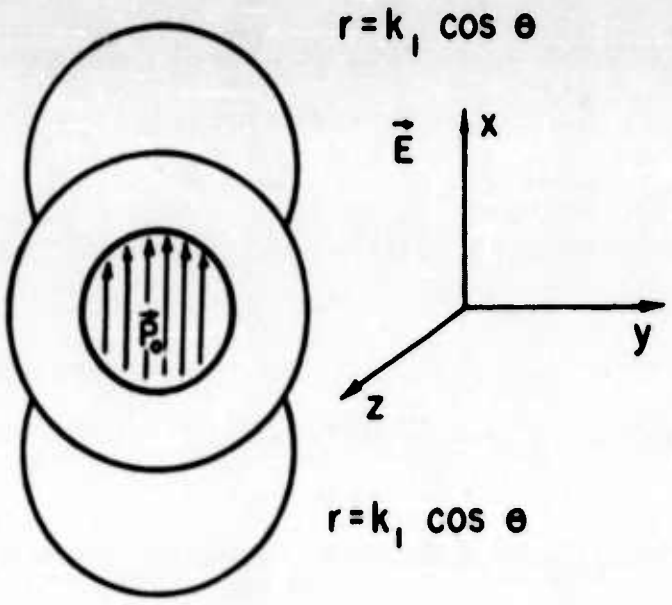

Fig. 5.3. Orientation of Crystal Axes With Respect to the Electrodes

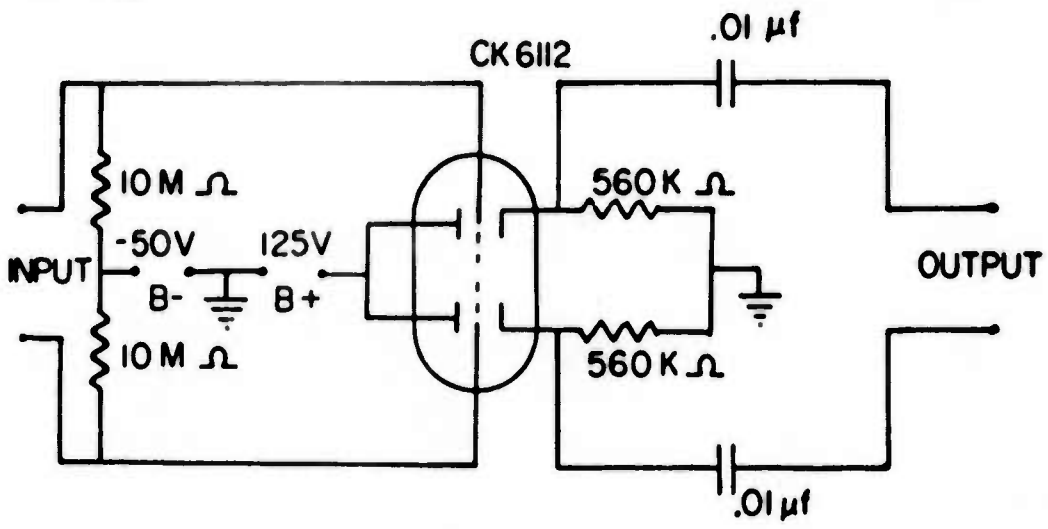

Fig. 5.4. Preamplifier Circuit Diagram

is - 50V. The cathode resistors are 560 kilohms each and the grid leak resistors are 10 meghohms each. The large resistance at the input is to obtain a high input impedance and the large resistance in the cathode circuit to keep the plate current low.

The input capacitance of each section of the preamplifier is

$$C_{in} = C_{gp} + C_{gk}(1 - A) \tag{5.1}$$

where C_{gp} is the grid-to plate capacitance, C_{gk} is the grid to cathode capacitance and A the gain of the amplifier. In the present case A is very nearly unity and hence Eq. (5.1) can be approximated as

$$C_{in} = C_{gp} \tag{5.1a}$$

Looking into the amplifier from the electrode terminals, the input capacitance of the two sections add in series and thus present a net input capacitance of half the input capacitance of each section. The same is true for the wiring capacitance. Thus the balanced input arrangement has the additional advantage of reducing the input capacitance as seen by the quartz.

To reduce the noise figure of the tube, its filament is heated from a d.c. source. Besides, the tube is operated under heavy space charge conditions. For the values chosen in Fig. (5.4), the current under operating conditions is less than 100 microamperes. The noise output level of the preamplifier as measured is approximately 25 microvolts.

5.3. Laser

The laser used is of pulsed ruby type. The laser cavity is of elliptical cross-section with ruby placed at one of the foci and the

linear flash tube at the other. The input to the flash tube is about 720 joules delivered by a capacitor bank of 360 microfarads. The laser output energy from the ruby is approximately 3 joules and the duration of the pulse is approximately 400 microseconds. The ruby is 90° cut, i.e., the optic axis is perpendicular to the direction of propagation and hence the laser output is linearly polarized [11].

5.4. Experimental Arrangement

The general set-up of the experiment is shown in Fig. (5.5). All the components are mounted on a lathe bed optical bench. The laser output is passed through the quartz detector. The quartz detector mount has facility for vertical, transverse and rotational alignments. The beam emerging from the detector strikes a white background. The scattered light is picked up by a photomultiplier and is fed to one of the inputs of the dual beam oscilloscope (Tektronic Model 555). The quartz detector amplifier is connected to the power supply by means of a shielded cable. The output of the quartz detector is fed to the second input of the oscilloscope. Both traces of the oscilloscope are synchronized with the same trigger voltage that is fed to the laser unit. The oscilloscope is set for single sweep operation.

There are some important precautions that should be observed in performing the experiments. As will be seen in the later sections of this chapter the signal that is to be measured is less than 50 microvolts. At this low level extreme care is to be observed in reducing the noise pick-ups as much as possible. Thus all leads from the output of the quartz crystal through the preamplifier, upto the input of the oscilloscope should be balanced. The leads are to be well shielded and

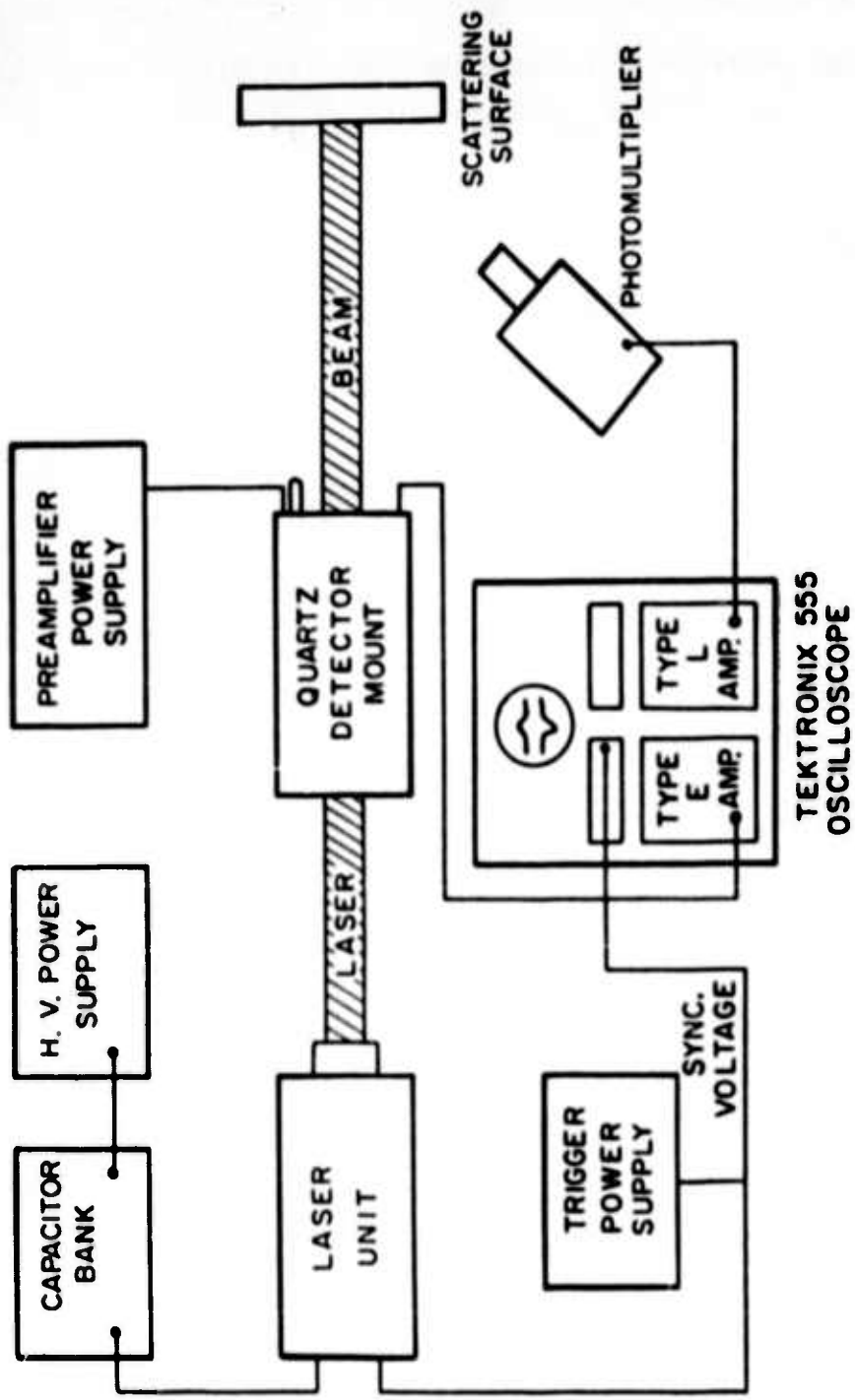

Fig 5.5. General Experimental Arrangement

and grounded. The grounding has to be one common ground. Any loops in the leads of the quartz detector is to be avoided to prevent any pick up of the radiation field set up by the high voltage trigger and the enormous current flow that occur during the firing of the flash tube. Also the laser power supply, the leads from it to the flash tube, the high voltage trigger and its leads, and the laser unit should all be well shielded. The appropriate precautions mentioned in Section 5.2 should be taken into account to keep down the preamplifier noise to the minimum extent possible.

The second important precaution that should be observed in conducting the experiments is the voltage that might be developed due to any phenomena other than the nonlinear polarization. One of the major sources will be the pyroelectric voltage. A detailed discussion on pyroelectricity can be found in the standard text books on crystals. It is enough to note here that the pyroelectric voltage is caused due to heating of the crystal and is developed in a unique direction of the crystal. In quartz crystal the pyroelectric coefficient is zero. However there may still be a small effect present due to impurities and imperfections in the crystal. The crystal should be free of strain and well polished. It should be mounted in such a manner as to introduce the least amount of strain. The sample used in the experiments described in the following sections, was found to have this abnormal voltage. It was reduced to a minimum by properly orienting the crystal with respect to the electrodes. This, of course would prevent the configuration described in Fig. (5.3). This presents no serious problem as the entire crystal mount can be rotated and positioned with respect to the polarization of the laser beam so as to produce the maximum

voltage on the electrodes.

Another precautionary step is to make sure that the beam is completely within the crystal and well centered. Extra precaution is to be observed in keeping the beam from hitting the electrodes.

5.5. Observation of d.c. Polarization

With the set-up shown in Fig. (5.5), the quartz output was measured. The output is of the order of 40 microvolts. This is for the angular position of the mount for which the output is positive maximum. Fig. (5.6a) is the oscilloscope picture showing this output. The upper trace is the photomultiplier output representing the laser output. The photomultiplier tube circuit has a long time constant and hence the spikes in the ruby output are not seen. Only the envelope of the laser output is present. The lower trace represents the quartz detector output at the position of maximum positive output. Fig. (5.6b) represents the situation when the quartz crystal is replaced by a glass rod. The angular position of the quartz mount is maintained the same as in the earlier case. The output of the quartz was due to its crystalline character. However glass is amorphous and should yield no output. Thus a comparison of the two output would prove that the output voltage is caused due to the crystalline nature of the medium. In Fig. (5.6b) one observes a very small output out of the glass rod which is found to be independent of the angular position. Thus this small output might be due to the residual strain in the glass rod.

One should expect the quartz detector output to be spiked since the laser output is. This follows from Section 3.3. The spikes are approximately spaced at time intervals of a microsecond and hence to

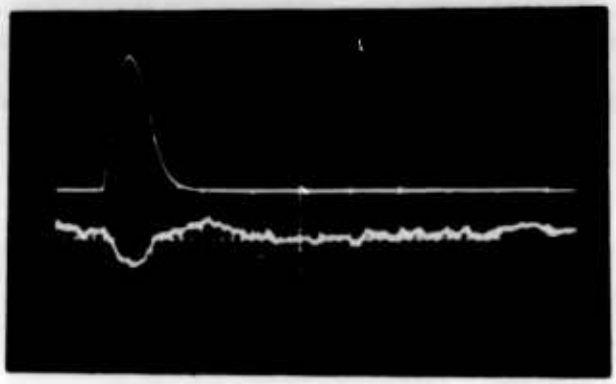

(a)

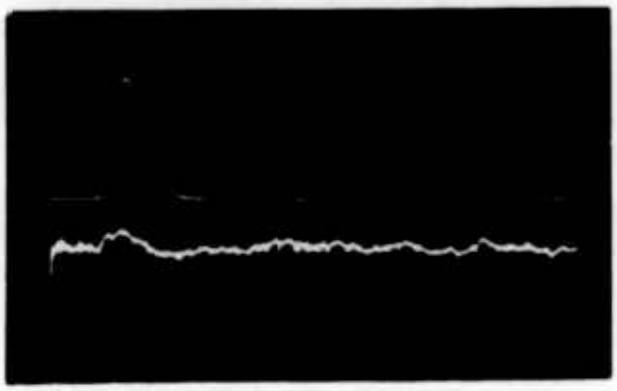

(b)

Fig. 5.6. Comparison of Output from Quartz Crystal with that from Glass Rod

(a) Photograph of the dual beam oscilloscope in which the lower trace shows the quartz detector output and the upper trace the intensity of the laser beam.
Sweep rate: 500 microseconds/cm.
Sensitivity of upper trace: 50 microvolts/cm.

(b) As in (a) with the quartz replaced by the glass rod.

detect them, the system should have a bandwidth in the order of at least megacycles. Since the output of the quartz detector is less than 50 microvolts, it is difficult to obtain a detector to measure such low voltage and at the same time to have a bandwidth of a few megacycles. The detecting system used is the Tektronix Model 555 oscilloscope with type E input amplifier. It has maximum sensitivity of 50 microvolts per centimeter with a bandwidth of 20 kilocycles. This is the reason for the inability to observe the spiking phenomenon.

5.6. Angular Dependence of d.c. Polarization

It was proved in Section 2.2 that rotating the quartz detector about its axis while keeping the electric field orientation of the laser beam fixed in space, the d.c. polarization should rotate at double the angular rate. Thus, if the quartz detector is rotated through 90° in either clockwise or anticlockwise direction the d.c. polarization vector should rotate through an angle of 180°. This means that one should expect a reversal in the d.c. output voltage of the quartz detector as it is rotated through 90°. This is proved by the pictures shown in Fig. (5.7). Fig. (5.7a) represents an angular position for which the output is a positive maximum. Fig. (5.7b) represents the angular position 90° away from that corresponding to Fig. (5.7a). It is seen that for the same laser power, depicted by the upper traces, the magnitude of the quartz output remains the same while the direction alone reverses.

For the same positions, the glass rod was tried and there was no reversal in output. The same output that is shown in Fig. (5.6b) was repeated thus proving that the small output from the glass is due to a

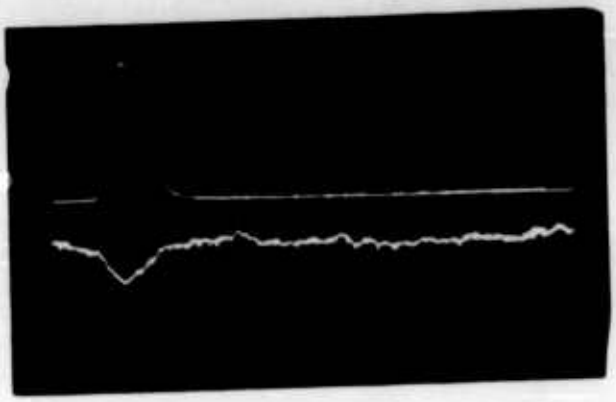

(a)

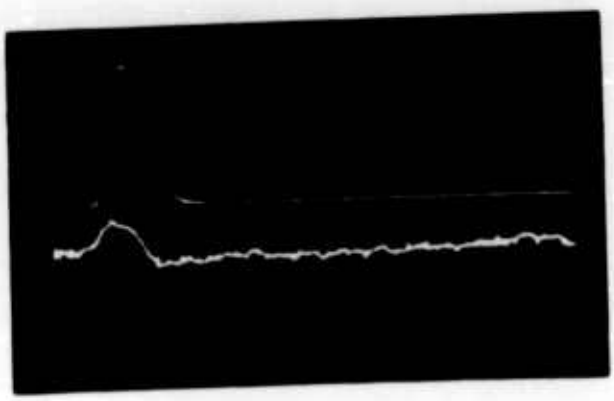

(b)

Fig. 5.7. Angular Dependence of d.c. Polarization

(a) Photograph of the dual beam oscilloscope in which the lower trace shows the quartz detector output and the upper trace the intensity of the laser beam. Quartz detector is adjusted for maximum negative output.

(b) As in (a); quartz detector rotated by 90° from that of position in (a).

phenomenon other than due to lack of inversion symmetry in a crystalline structure.

5.7. Determination of the Second Order Nonlinear Coefficient α

It is possible to establish the value of the second order nonlinear coefficient α in the matrix of Eq. (2.2) by measuring the d. c. output voltage of the quartz detector. The procedure is to first determine the peak power in the laser pulse by measuring the total energy using calorimetric technique and knowing the pulse shape given by the photomultiplier output. Substituting this value of the peak power and the value of the capacitances in Eq. (4.36), one can calculate the coefficient K_2. Knowing K_2, α can then be obtained by using Eq. (4.35).

The laser energy was measured with the rat's nest calorimeter that was specially constructed for the purpose. The energy output of the laser was found to be 3 joules for an input energy of 720 joules. Since the photomultiplier output is directly proportional to the instantaneous light intensity, the amplitude of the photomultiplier output directly indicates the relative instantaneous power in the laser beam. Thus the energy of 3 joules corresponds to the area under the laser pulse represented by the upper traces of the pictures in Figs. (5.6) and (5.7). From these data, the peak power of the laser pulse can be shown to be equal to 15 kilowatts.

To calculate C_Q', the capacitance of the quartz crystal with the special electrodes, one can make an approximate estimate of the same by the method suggested in the appendix. The actual cross section of the crystal and the electrodes and their lengths are shown in Fig. (5.8).

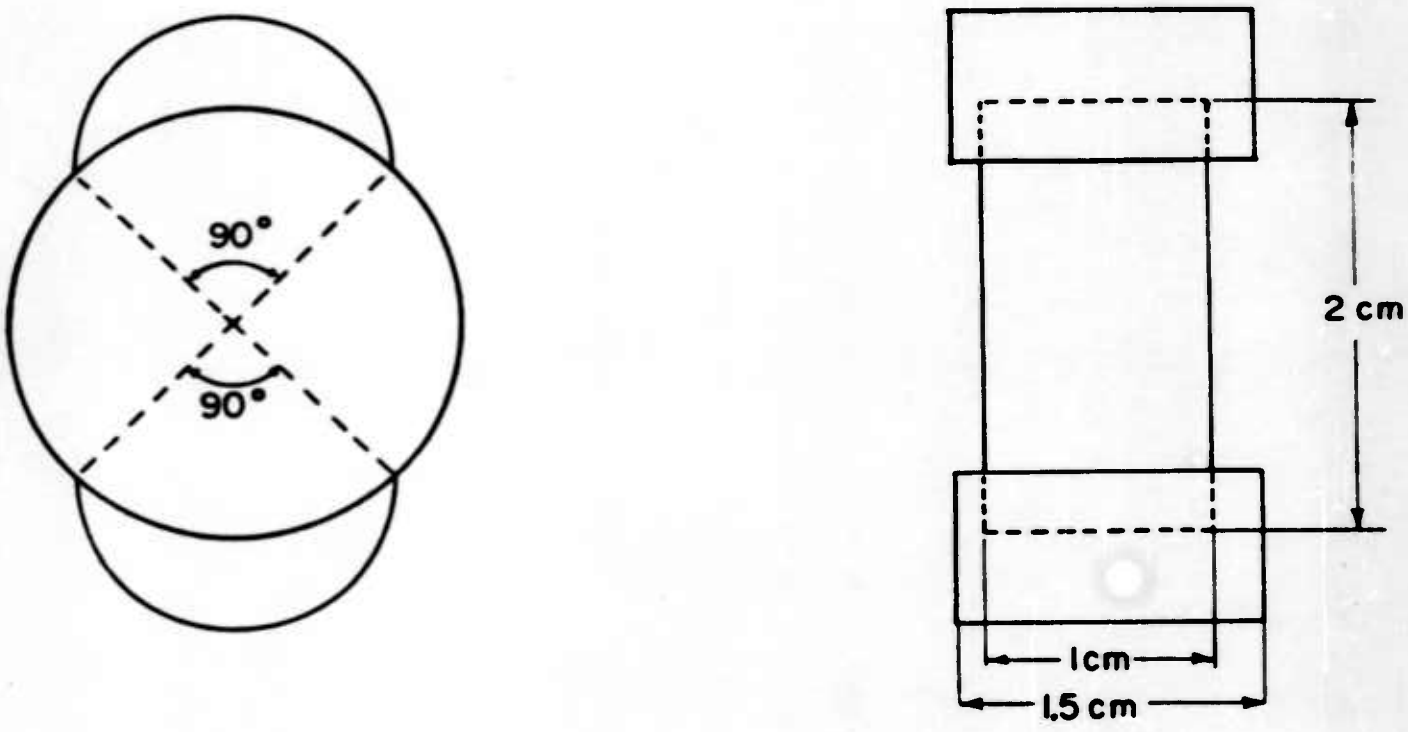

Fig. 5.8. Crystal and Electrode Assembly Dimensions

This is approximated with the configuration shown in Fig. (A.1) of the appendix. The capacitance is then given by Eq. (A.33) which is re-written below.

$$C_Q' = \epsilon_o \ell (\epsilon_r + 1) \tag{5.2}$$

Substituting the following values in Eq. (5.1a)

$$\epsilon_o = \frac{1}{36\pi} \times 10^{-9}$$

$$\epsilon_r = 4.5$$

and

$$\ell = 1.5 \text{ cm.}$$

one obtains for the capacitance an approximate value

$$C_Q' = 0.75 \text{ pf} \tag{5.3}$$

The actual measured value is 0.9 pf.

Because of the approximation made in the configuration of the plates with respect to the crystal in the above derivation, one has in Eq. (3.25)

$$C_Q = C_Q' \tag{5.4}$$

Hence Eq. (3.25) reduces to

$$V_e = V_Q \tag{5.5}$$

An estimate could easily be made of the input capacitance C pre-

sented by the preamplifier. This is given by Eq. (5.1) plus the stray capacitance. From the tube manual one has for the tube grid to plate capacitance a value in the range of 1.0 pf. The stray capacitance for each stage can be assumed to be in the order of 9 pf. Thus the total input capacitance presented by each section is in the order of 10 pf. The input capacitance of the two sections are to be added in series to calculate the total input capacitance in Eq. (4.36). It is in the order of 5 pf. The actual measured value is 7.1 pf. Substituting C_Q, C_Q' and C in Eq. (4.36) one has for the peak output voltage

$$V_{o_{max}} = \frac{K_2}{8.9} P_{L_{max}} \tag{5.7}$$

Substituting

$$P_{L_{max}} = 15 \times 10^3$$

one obtains

$$K_2 = \frac{V_{o_{max}}}{1.7 \times 10^3} \tag{5.8}$$

The relationship between K_2 and α can be obtained by substituting the following values for the newly encountered variables in Eq. (4.35)

$$k_1 = \sqrt{2}\, b$$

$$b = 1 \text{ cm}$$

$$\eta = 80\pi$$

Then

sented by the preamplifier. This is given by Eq. (5.1) plus the stray capacitance. From the tube manual one has for the tube grid to plate capacitance a value in the range of 1.0 pf. The stray capacitance for each stage can be assumed to be in the order of 9 pf. Thus the total input capacitance presented by each section is in the order of 10 pf. The input capacitance of the two sections are to be added in series to calculate the total input capacitance in Eq. (4.36). It is in the order of 5 pf. The actual measured value is 7.1 pf. Substituting C_Q, C_Q' and C in Eq. (4.36) one has for the peak output voltage

$$V_{o_{max}} = \frac{K_2}{8.9} P_{L_{max}} \tag{5.7}$$

Substituting

$$P_{L_{max}} = 15 \times 10^3$$

one obtains

$$K_2 = \frac{V_{o_{max}}}{1.7 \times 10^3} \tag{5.8}$$

The relationship between K_2 and α can be obtained by substituting the following values for the newly encountered variables in Eq. (4.35)

$$k_1 = \sqrt{2}\, b$$

$$b = 1 \text{ cm}$$

$$\eta = 80\alpha$$

Then

$$\alpha = 4.3 \times 10^{-15} K_2 \tag{5.9}$$

From Eqs. (5.8) and (5.9)

$$\alpha = 2.5 \times 10^{-18} V_{o_{max}} \quad \text{m.k.s. units} \tag{5.10}$$

The conversion from m.k.s. units to c.s. units can be shown to be

$$1 \text{ e.s.u.} = \frac{10^{-14}}{2.73} \quad \text{m.k.s. units} \tag{5.11}$$

From Eqs. (5.10) and (5.11), α in e.s.u. is given by

$$\alpha = 6.8 \times 10^{-4} V_{o_{max}} \text{ e.s.u.} \tag{5.12}$$

The experimentally $V_{o_{max}}$ is about 40 microvolts. This yields a value for α

$$\alpha = 2.72 \times 10^{-8} \text{ e.s.u.} \tag{5.13}$$

It was pointed out in Section 1.2 that the second order polarization tensor is the same as the linear electro-optic tensor. The value of α from the tables of linear electro-optic tensor is 1.4×10^{-8} e.s.u. One finds from Eq. (5.13) that the estimate on α from the experiment described is approximately twice the theoretical value. This is well within the experimental errors of the present set-up.

5.8. Influence of Radius of the Beam on d.c. Voltage Output

It was shown in Section 4.3 that the voltage output of the quartz

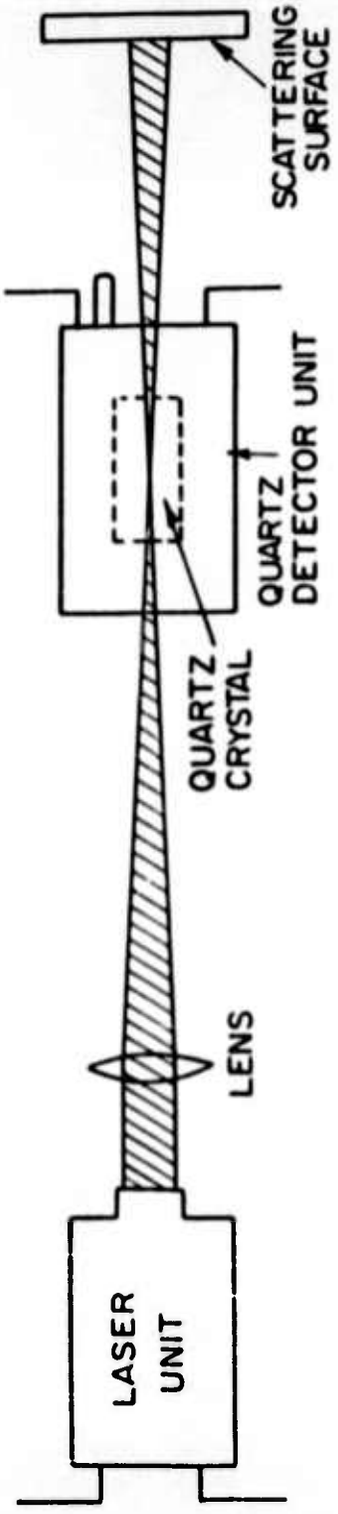

Fig. 5.9. Experimental Arrangement for Verifying Focusing Effect

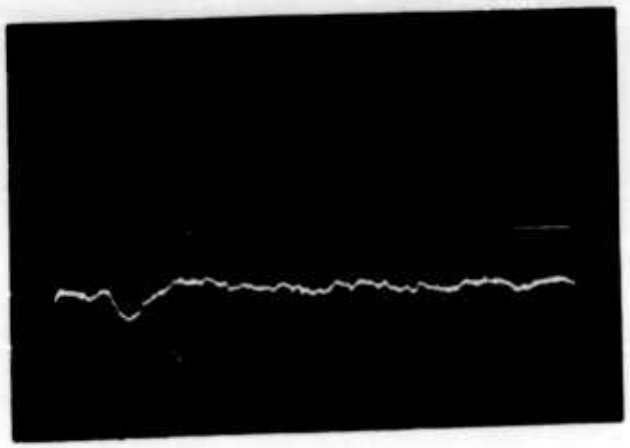

(a)

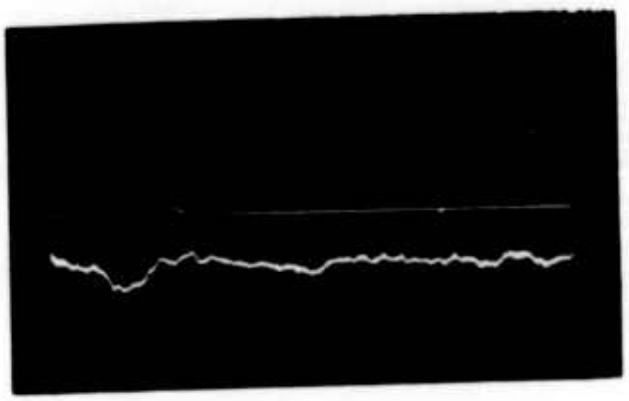

(b)

Fig. 5.10. Comparison of Quartz Detector Output due to Focused Laser Beam with that of Non-focused Beam

(a) Photograph of the dual beam oscilloscope in which the lower trace shows the quartz detector output and the upper trace the intensity of the laser beam; the case of the focused laser beam.

(b) As in (a); the case of unfocused laser beam.

detector due to d.c. polarization is independent of the radius of the beam provided the intensity of the beam remains constant and provided also the beam is completely contained within the crystal. Thus any focusing or defocusing of the beam should not have any influence on the quartz detector output. This was verified with the set-up shown in Fig. (5.9). A lens is placed between the laser and the quartz detector. In order to contain the beam completely within the crystal, the focal length of the lens should be long. The lens that was used in the experiment had a focal length of 19 cms. The results are shown in Fig. (5.10). Fig. (5.10a) represents the case without lens and Fig. (5.10b) the situation when the lens is inserted in the path. The beam is focused to a point at the center of the axis of the crystal. It can be seen that focusing of the beam has no effect on the output of the quartz detector, thus confirming the theory of Section 4.3.

5.9. Relation Between d.c. Polarization and Laser Power Intensity

In Chapter 4 a method was suggested to determine the intensity of laser beam by measuring the d.c. polarization. With the experimental set-up shown in Fig. (5.5), this was proved by observing the peak d.c. output of the quartz detector for various peak intensities of the laser pulse. The peak values were compared so as to obtain greater accuracies as the intensity of the laser beam was not high enough. In Fig. (5.11) three representative pictures are given that show the linear relationship between the quartz detector output and the laser output. The upper traces, as before, represent the photomultiplier output and the lower traces the quartz detector output. As the photomultiplier

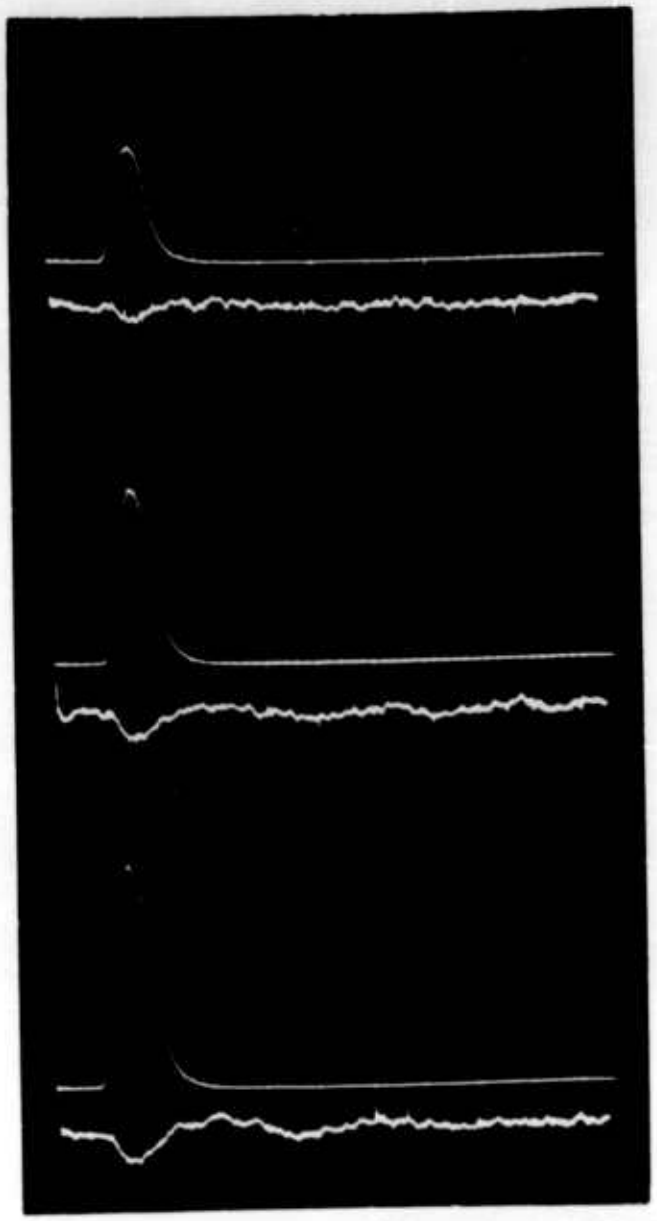

Fig. 5.11. Dependence of d.c. Polarization on Laser Beam Intensity; Photographs of the dual beam Oscilloscope in which the lower trace shows the quartz detector output and the upper trace the intensity of the laser beam

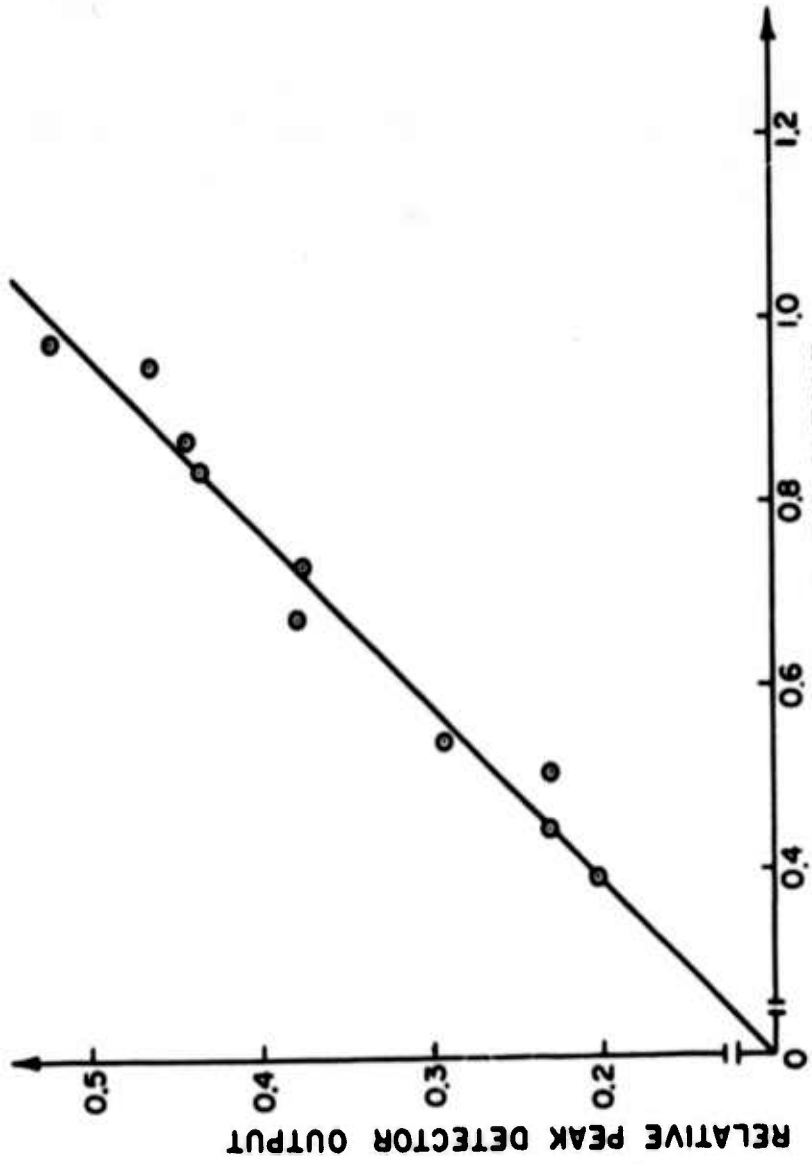

Fig. 5.12. Peak Detector Output vs. Peak Laser Power Output

measures the intensity of the light, its output is directly proportional to the intensity of the laser beam. Fig. (5.12) shows the results in the graphical form. It can be observed that the graph is linear, thus establishing the feasibility of using the idea as a power meter.

Chapter 6

SUMMARY OF RESULTS AND CONCLUSIONS

The d.c. polarization that is developed in a nonlinear dielectric medium when a high intensity laser beam propagates through is investigated. Crystalline quartz, belonging to class 32 that lacks inversion symmetry is chosen as the nonlinear dielectric medium. By a simple mathematical approach, the relationship between laser intensity and the d.c. polarization is established for two cases of propagation. It is found that for the case of propagation along z-axis, the d.c. polarization is directly proportional to the intensity of the laser beam. The d.c. polarization is zero if the laser beam is circularly polarized.

A convenient method to detect the d.c. polarization is suggested. The interaction between the propagating wave and the detecting circuitry has been analyzed and an equivalent circuit model has been developed. It is proved that the phenomenon of d.c. polarization cannot transfer any power from optical frequency to d.c. However, it can deliver power to the detecting circuit if the laser beam is modulated. Thus, the spikes in the laser pulse should be observable by the detecting circuitry.

A theoretical analysis is presented on the feasibility of using this phenomenon for power measurement of high power lasers. A practical method of constructing the device is given.

Due to lack of a high power laser, only the following theoretical results is verified experimentally. The laser used is a ruby laser whose output pulse has a duration of 400 microseconds and contains an energy of 3 joules. The presence of a d.c. polarization is established. By measurement of this d.c. polarization, one of the two elements of the second order polarization coefficient is estimated to be approximately 2.7×10^{-8} e.s.u. which is in agreement within a factor of two with the theoretical value of 1.4×10^{-8} e.s.u. The error is mainly attributed to the difficulty in measuring the low level d.c. output pulse which has a peak amplitude of approximately 40 microvolts.

The linear relationship between the laser intensity and the d.c. voltage output of the quartz detector is verified. This d.c. output is found to be independent of the area of cross-section of the beam provided the intensity remains constant. Also there is very little power loss to the circuitry. However, the above attractive advantages for using this phenomenon for power measurement are somewhat hindered by the following disadvantages. The beam needs to be centered and also needs to be of circular cross-section for the cylindrical crystal chosen.

From the above results the following conclusions are made. There exists the phenomenon of nonlinear d.c. polarization in quartz crystal. By measurement of this d.c. polarization using suitable detecting technique, an estimate of the second order nonlinear polarization coefficient could be made. The experimental results are in agreement with the theoretical prediction made by Armstrong, et. al., that the second order polarization coefficient tensor is the same as the electro-optic tensor. The practicability of using this principle for power measurement needs

further study for general usability with all types of pulsed lasers.

The future course of work is recommended to be pursued in the following direction. Using a higher power laser, correspondence between the spikes of laser and spikes of the d.c. polarization is to be established. Studies on other crystals can be made with a view of selecting good crystals for second harmonic generation.

BIBLIOGRAPHY

1. P. A. Franken, A. E. Hill, C. W. Peters and G. Weinreich, "Generation of Optical Harmonics," Phys. Rev. Letters, Vol. 7, No. 4, pp. 118-119, August 15, 1961.

2. J. A. Giordamine, "Mixing of Light Beams in Crystals," Phys. Rev. Letters, Vol. 8, pp. 19-20, January, 1962.

3. P. D. Maker, R. W. Terhune, M. Nisenoff and C. M. Savage, "Effects of Dispersion and Focussing on the Production of Optical Harmonics," Phys. Rev. Letters, Vol. 8, pp. 21-22, January 1962.

4. M. Bass, P. A. Franken, J. F. Ward and G. Weinreich, "Optical Rectification," Phys. Rev. Letters, Vol. 9, No. 11, pp. 446-448, December 1, 1962.

5. P. A. Franken and J. F. Ward, "Optical Harmonics and Nonlinear Phenomena," Revs. Mod. Phys., Vol. 35, No. 1, pp. 23-39, January 1963.

6. "Standards on Piezoelectric Crystals," Proc. I. R. E., Vol. 46, p. 764, (1958).

7. J. A. Armstrong, N. Bloembergen, J. Ducing and P. S. Pershan, "Interactions between Light Waves in a Nonlinear Dielectric," Phys. Rev., Vol. 127, No. 6, pp. 1918-1939, September 15, 1962.

8. P. S. Pershan, "Nonlinear Optical Properties of Solids: Energy Considerations," Phys. Rev., Vol. 130, No. 3, pp. 919-929, May 1, 1963.

9. J. F. Nye, "Physical Properties of Crystals," Oxford Press, p. 116; (1957).

10. W. K. H. Panofsky and M. Philips, "Classical Electricity and Magnetism," Addison-Wesley Pub. Co., p. 143; (1956).

11. D. F. Nelson and R. J. Collins, "The Polarization of the Output from a Ruby Optical Maser," Advances in Quantum Electronics, Columbia University Press, p. 79; (1961).

12. J. Hodgkinson, "A Note on a Two-dimensional Problem in Electrostatics," Quar. Jour. Math., Oxford series, Vol. 9, pp. 5-13, (1938).

13. Zeev Nehari, "Conformal Mapping," McGraw-Hill Book Co., pp. 281-282; (1952).

Appendix

A.1. Outline of the Procedure

Fig. (A.1) shows the cross-section of a quartz rod with two conducting plates AB and CD symmetrically placed on it. The radius of the rod is assumed to be unity and it is assumed to be of infinite length. The problem is to calculate the capacitance of this configuration. Since the rod and the conducting plates are of infinite length, the problem can be treated as a two-dimensional case. However, the complications arise because of the mixed boundary conditions. The problem can be reduced to that of a parallel plate capacitance by making the appropriate conformal transformations as suggested by Hodgkinson [12]. The procedure is to transform the interior of the circle enclosed by the arcs AB and CD in the z-plane into the upper half of the v-plane by making use of a suitable linear transformation. The points A, B and C in the z-plane are transformed into points e_1, e_2 and e_3 along the real axis of the v-plane such that $e_1 + e_2 + e_3 = 0$. The point D in the z-plane is transformed into the point ∞ in the v-plane. This is shown in Fig. (A.2). Then a two-sheeted surface is formed by adjoining a lower sheet in which the lower half of the sheet is filled with the dielectric, connection between the sheets being through the branch lines AB and CD. This is represented in Fig. (A.3). This surface is then transformed into ξ-plane by using the elliptic function

$$v = \wp(\xi) \qquad (A.1)$$

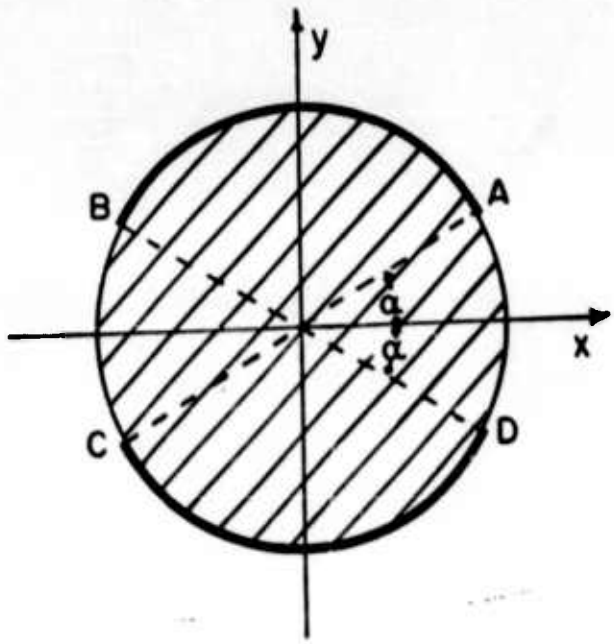

Fig. A.1. Configuration in the z-plane

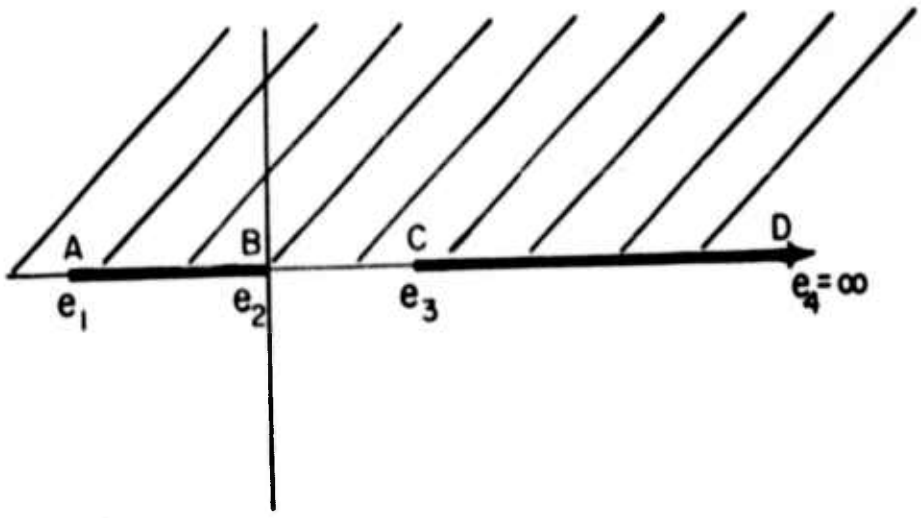

Fig. A.2. Configuration in the w-plane Obtained by Linear Transformation of Fig. (A.1)

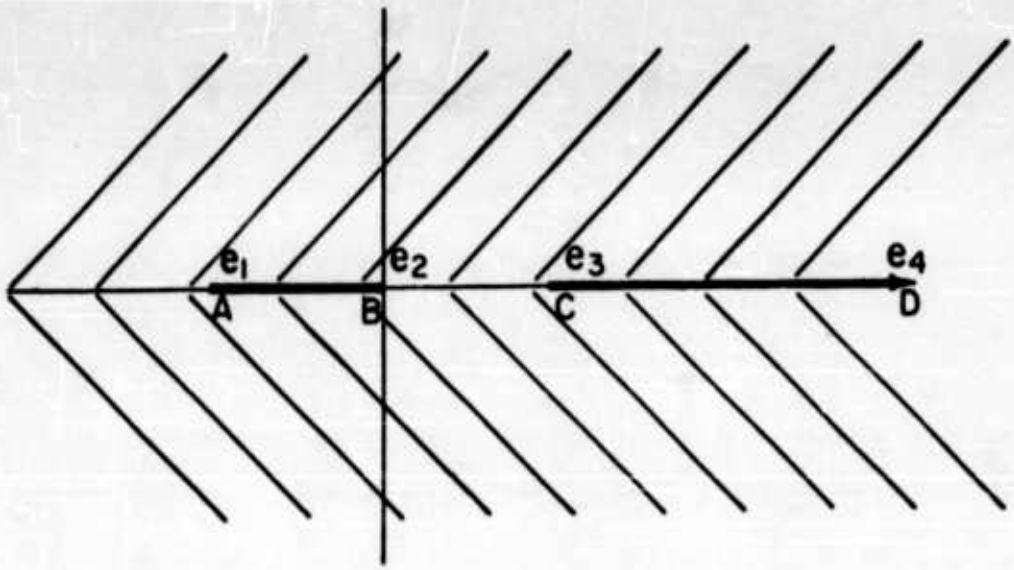

Fig. A.3. Two Sheeted Surface in the w-plane Obtained by Adding to Fig. (A.2), Its Complimentary Part

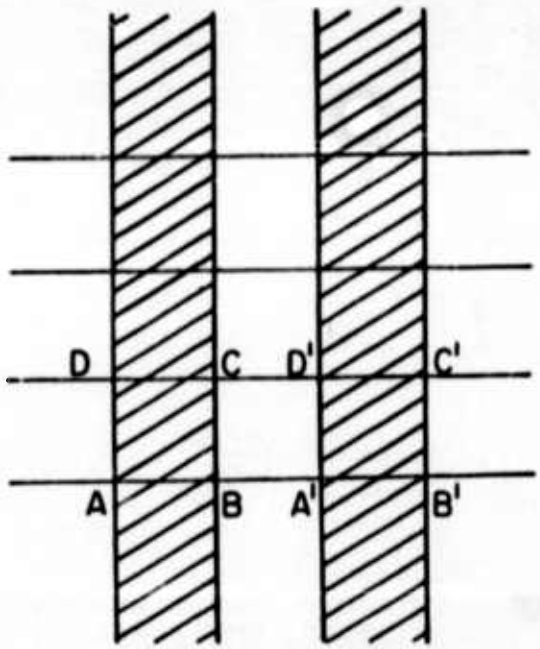

Fig. A.4. Configuration in the ξ-plane Obtained by Using the Elliptic Function $w = \wp(\xi)$

where

$$\wp'(\xi) = 4\pi[\wp(\xi) - e_r] \qquad (r = 1, 2, 3) \tag{A.2}$$

The ξ-plane is divided into rectangles as shown in Fig. (A.4) with the real and purely imaginary periods of the elliptic functions ω_r and ω_i respectively. The lines with imaginary part of ξ = constant are equipotential lines. Thus the problem reduces to that of a parallel plate capacitance. All conditions are satisfied if one places a charge $2\epsilon_o\rho$ along BA' and all lines congruent to it in the configuration of period parallelograms, $2\epsilon\rho$ along AB and congruent lines, $-2\epsilon_o\rho$ along CD' and congruent lines and $-2\epsilon\rho$ along DC and congruent lines. Here ϵ_r is the relative dielectric constant of the material, ϵ_o the free space permittivity and $\epsilon = \epsilon_o\epsilon_r$. It has been shown [11] that this is equivalent to placing these charges per unit length in the original problem. One can now easily calculate the capacitance of the system per unit length.

A.2. Transformation from z-plane to w-plane

The linear transformation is given by

$$\frac{(w - w_1)(w_2 - w_3)}{(w - w_3)(w_2 - w_1)} = \frac{(z - z_1)(z_2 - z_3)}{(z - z_3)(z_2 - z_1)} \tag{A.3}$$

From Fig. (A.1) one has

$$\begin{aligned} A &= z_1 = e^{i\alpha} \\ B &= z_2 = -e^{-i\alpha} \\ C &= z_3 = -e^{i\alpha} \\ D &= z_4 = e^{-i\alpha} \end{aligned} \tag{A.4}$$

Let z_1, z_2 and z_4 be transformed to points e_1, e_2 and ∞ in the v-plane. Then the corresponding points in Eq. (A.3) are given by

$$\begin{aligned} z_1 &= e^{i\alpha} \quad \dots \quad v_1 = e_1 \\ z_2 &= -e^{-i\alpha} \quad \dots \quad v_2 = e_2 \\ z_4 &= e^{-i\alpha} \quad \dots \quad v_4 = \infty \end{aligned} \tag{A.5}$$

Substituting Eq. (A.5) in Eq. (A.3) one obtains

$$v = \frac{z\left[2e_2 - e_1 + e_1 e^{i2\alpha}\right] + \left[e_1 e^{i\alpha} - 2e_2 e^{i\alpha} - e_1 e^{i\alpha}\right]}{z\left[1 + e^{i2\alpha}\right] - \left[e^{i\alpha} + e^{-i\alpha}\right]} \tag{A.6}$$

Now substituting the value of z_3 from Eq. (A.4) in Eq. (A.6), one has for $v_3 = e_3$ the following equation.

$$e_3 = \frac{e_1[-2 + 2\cos 2\alpha] + 4e_2}{2 + 2\cos 2\alpha} \tag{A.7}$$

The required condition between e_1, e_2 and e_3 is

$$e_1 + e_2 + e_3 = 0 \tag{A.8}$$

Using Eqs. (A.7) and (A.8), e_2 and e_3 can be expressed in terms of e_1. Thus

$$e_2 = \frac{-2\cos 2\alpha}{3 + \cos 2\alpha} e_1 \tag{A.9}$$

$$e_3 = \frac{\cos 2\alpha - 3}{\cos 2\alpha + 3} e_1 \tag{A.10}$$

If one chooses $e_1 = -1$, then from Eqs. (A.6) and (A.9), the required transformation is

$$w = \frac{z\left[-e^{i4\alpha} - e^{i2\alpha} + 5e^{-i2\alpha} + 5\right] + \left[-5e^{i3\alpha} + e^{-i3\alpha} - 5e^{i\alpha} + e^{i\alpha}\right]}{z\left[e^{i4\alpha} + 7e^{i2\alpha} + e^{i2\alpha} + 7\right] - \left[e^{i3\alpha} + e^{-i3\alpha} + 7e^{i\alpha} + 7e^{-i\alpha}\right]} \tag{A.11}$$

and the values for e_1, e_2, e_3 and e_4 are

$$\begin{aligned} e_1 &= -1 \\ e_2 &= \frac{2\cos 2\alpha}{3 + \cos 2\alpha} \\ e_3 &= \frac{3 - \cos 2\alpha}{3 + \cos 2\alpha} \\ e_4 &= \infty \end{aligned} \tag{A.12}$$

A.3. Transformation from w-plane to ξ-plane

The elliptic function that is used for the transformation can be written in the Schwarz-Christoffel form as

$$t = A \int_0^w \frac{dw}{(w - e_1)^{1/2} (w - e_2)^{1/2} (w - e_3)^{1/2}} \tag{A.13}$$

Let

$$w - e_1 = x^2 \tag{A.14}$$

Then

$$dw = 2x\, dx \tag{A.15}$$

Substituting Eqs. (A.14) and (A.15) in Eq. (A.13), one has after rearrangement

$$\xi = \frac{2A}{(e_2 - e_1)^{1/2}\,(e_3 - e_1)^{1/2}} \int_0^x \frac{dx}{\left[\frac{x^2}{(e_2-e_1)} - 1\right]^{1/2} \left[\frac{x^2}{(e_3-e_1)} - 1\right]^{1/2}} \tag{A.16}$$

Now, let

$$\frac{x}{(e_2 - e_1)^{1/2}} = \lambda \quad ; \quad dx = (e_2 - e_1)^{1/2}\, d\lambda \tag{A.17}$$

Using Eq. (A.17), Eq. (A.16) can be rewritten as

$$\xi = L \int_0^\lambda \frac{d\lambda}{(1 - \lambda^2)^{1/2}\,(1 - k^2\lambda^2)^{1/2}} \tag{A.18}$$

where

$$L = -\frac{2A}{(e_3 - e_1)^{1/2}} \tag{A.19}$$

and

$$k^2 = \frac{e_2 - e_1}{e_3 - e_1} \tag{A.20}$$

From Eqs. (A.9), (A.10) and (A.19)

$$k^2 = \frac{\cos 2\alpha}{2} + \frac{1}{2} \leq 1 \qquad (A.21)$$

Eq. (A.18) can be recognized as the elliptic integral of the first kind. It has two periods, designated by ω_r and ω_i along the real and imaginary axes respectively. The transformed configuration is shown in Fig. (A.4). Here $AB = BA' = \omega_r$ and $BC = \omega_i$. The values of ω_r and ω_i can be read from the table of elliptic integrals knowing e_1, e_2, and e_3.

A.4. Calculation of the Capacitance

As mentioned in Section (A.1), $ABA'B'$ and $DCD'C'$ are equipotential lines. Hence they can be considered as conducting surfaces. They form a parallel plate capacitance. The two-dimensional condition is satisfied by assuming the plates to be extending to infinity in the direction perpendicular to the plane of the paper. Let $2\epsilon_o\rho$ be the charge density on BA' and $2\epsilon\rho$ on AB and similarly $-2\epsilon_o\rho$ on CD' and $-2\epsilon\rho$ on DC. One has to remember that only half of these charges are to be taken into account in calculating the capacitance since the other half is due to the adjacent capacitor. Thus the charge on ABA' is

$$Q_+ = \omega_r \epsilon_o (1 + \epsilon_r)\rho \qquad (A.22)$$

The charge on DCD' is

$$Q_- = -\omega_r \epsilon_o (1 + \epsilon_r)\rho \qquad (A.23)$$

The capacitance per unit length (the length being taken perpendicular to the plane of the paper) is

$$C_\ell = \frac{\epsilon_o \omega_r(\epsilon_r + 1)}{\omega_1} \qquad (A.24)$$

In describing Eq. (A.4) the radius has been taken as equal to unity. This normalization however, does not affect the final result since the magnitude of the radius multiplies ω_r and ω_i by the same quantity and hence gets cancelled in the calculation of the capacitance using Eq. (A.24).

The capacitance for the specific case where $\alpha = 45^\circ$ (the value used in the experimental set up of this work) will now be calculated. Eq. (A.4) give the coordinates of A, B, C and D in the z-plane as

$$\begin{aligned} A &= z_1 = e^{i\pi/4} \\ B &= z_2 = -e^{-i\pi/4} \\ C &= z_3 = -e^{i\pi/4} \\ D &= z_4 = e^{-i\pi/4} \end{aligned} \qquad (A.25)$$

Assuming $e_1 = -1$ that corresponds to the point A in the w-plane, the coordinates of A, B, C and D in the w-plane can be written by making use of Eqs. (A.12).

$$\begin{aligned} e_1 &= -1 \\ e_2 &= 0 \\ e_3 &= +1 \\ e_4 &= \infty \end{aligned} \qquad (A.26)$$

One need not calculate the coordinates of the point A, B, C and D in the ξ-plane, since only the two periods are of interest here. They are

given by [13]

$$\omega_r = L \int_0^1 \frac{d\lambda}{(1 - \lambda^2)^{1/2} (1 - k^2\lambda^2)^{1/2}} \tag{A.27}$$

$$\omega_i = L \int_0^1 \frac{d\lambda}{(1 - \lambda^2)^{1/2} (1 - k'^2\lambda^2)^{1/2}} \tag{A.28}$$

where

$$k' = (1 - k^2)^{1/2} \tag{A.29}$$

For $\alpha = 45^\circ$, one observes from Eqs. (A.21) and (A.29) that

$$(k')^2 = (k)^2 = \frac{1}{2} \tag{A.30}$$

Thus

$$\omega_r = \omega_i \tag{A.31}$$

and from Eq. (A.24) the capacitance per unit length is given by

$$C_\ell = \epsilon_o(\epsilon_r + 1) \tag{A.32}$$

If the length of the plates is designated by l, then the capacitance of the quartz detector, neglecting the fringe effects is given by

$$C_Q = \epsilon_o \ell(\epsilon_r + 1) \tag{A.33}$$

VITA

Mahadevan Subramanian, a citizen of India, [redacted]. He completed the high school education in April 1949 and entered the Government Arts College, Madras from where he received the B. Sc. (Phys) degree in April 1953. He continued his education at Madras Institute of Technology, Madras. He received the Dip. M.I.T. (Electronics) from the Madras Institute of Technology in May 1956. After a three-year break in studies he joined Purdue University in September, 1959. He obtained the M.S.E.E. degree in January 1961 and decided to pursue at the University a course of study leading to the doctorate in Electrical Engineering.

Between July and December 1956 he was in-charge of the radio assembly section in G. Janshi and Company, Madras. Having been selected for training in radio broadcasting, he joined the All India Radio, New Delhi in January, 1957. After the six-month training he accepted a research job with Central Electronics Engineering Research Institute, Pilani, Rajasthan, India. During his stay of two years there, he was working in the field of microwave receivers. He left India in August 1959 to pursue further studies at Purdue University. While studying at Purdue University, he was a member of the staff in various positions.

M. Subramanian is a member of Sigma Pi Sigma and a student member of I.E.E.E.

RECENT RESEARCH PUBLICATIONS
SCHOOL OF ELECTRICAL ENGINEERING
PURDUE UNIVERSITY

TR-EE63-1 **ESTIMATION OF TIME-VARYING CORRELATION FUNCTIONS**

G. R. Cooper, Principal Investigator, H. Berndt, NSF Contract G-18997, March, 1963.

TR-EE63-2 **ADVANCED COMMUNICATION THEORY TECHNIQUES**

J. C. Hancock, Principal Investigator, D. G. Lainiotis, J. C. Lindenlaub, R. G. Marquart, H. Schwarzlander, Contract AF 33(657)-7410, (PRF 3040), March, 1963.

TR-EE63-3 **SINGULAR SOLUTIONS IN PROBLEMS OF OPTIMAL CONTROL**

J. E. Gibson, Principal Investigator, C. D. Johnson, NSF G-16460, (PRF 2743), August, 1963.

TR-EE63-4 **IMPROVEMENT IN PULSE TRANSMISSION ON COAXIAL TRANSMISSION LINES BY REDUCTION OF SKIN EFFECT**

C. M. Evans, Principal Investigator, L. R. Wheeler, Contract No. I.V-1163-1 Sub/w AT(29-1)-1183, (PRF 3535), September, 1963.

TR-EE63-5 **ANALYSIS OF WORST CASE BEHAVIOR IN FORCED CONTROL SYSTEMS.**

J. E. Gibson and Z. V. Rekasius, Principal Investigators, D. R. Howard and R. Mukundan, Contract No. AF 29(600)-2566, PRF #2304, September, 1963.

TR-EE63-6 **SUB-OPTIMAL CONTROL AND STABILITY OF NON-LINEAR FEEDBACK SYSTEMS**

J. E. Gibson and Z. V. Rekasius, Principal Investigators, E. S. Ibrahim, R. L. Haussler, and R. Mukundan, Contract No. AF 29(600)-2566, PRF #2304, September, 1963

TR-EE63-7 **PHILOSOPHY AND STATE OF THE ART OF LEARNING CONTROL SYSTEMS**

J. E. Gibson and K. S. Fu, Principal Investigators, with J. D. Hill, J. A. Lunst, R. H. Raible, and M. D. Waltz, Contract No. AF AFOSR 62-251, PRF #3123, (AF Report No. AFOSR 5144), November, 1963.

TR-EE63-8 **THE SCATTERING OF ELECTROMAGNETIC WAVES BY PERFECTLY REFLECTING OBJECTS OF COMPLEX SHAPE**

F. V. Schultz, D. M. Rolle and J. K. Schindler, Final Report, Contract No. AF 19(604)-4051, PRF #1947, January 1963.

TR-EE63-9 **ON A CLASS OF TRANSMITTED REFERENCE SYSTEMS FOR COMMUNICATION IN RANDOM OR UNKNOWN CHANNELS**

J. C. Hancock, Principal Investigator, Gopichand D. Hingorani, Contract NSF G-18997, (PRF 2974), December 1963.

TR-EE64-1 **FINITE TIME AVERAGE ESTIMATES OF NONSTATIONARY AUTOCORRELATION FUNCTIONS.**

C. R. Cooper, Principal Investigator, R. L. Mitchell, Contract NSF G-18997, (PRF 2974), January 1964.

TR-EE64-2 **ESTIMATION OF RADAR TARGET PARAMETERS FROM REFLECTED RANDOM SIGNALS**

G. R. Cooper, Principal Investigator, Michael P. Grant, Contract NSF G-18997, (PRF 2974), February 1964.

TR-EE64-3 **NONLINEAR FREQUENCY CONVERTERS.**

B. J. Leon, Principal Investigator, Contract NSF GP-981, PRF 3426-50-780, February 1964.

(Continued on outside back cover)